Characterization of Neuronal Ceroid Lipofuscinosis Phenotype in Three Different Cell Lines Subjected to RNA interference

Mari Tervaniemi

Department of Biological and Environmental Science

Faculty of Mathematics and Science

University of Jyväskylä

PREFACE

"Failure is success if you learn from it." -Malcolm Forbes

This master's thesis study was carried out at National Public Health Institute, Department of molecular medicine, Disease mechanisms research group, in collaboration with FIMM, Finnish Institute of Molecular Medicine.

I would first like to thank the group leader Anu Jalanko for giving me the opportunity to continue working as a master's thesis student after my practical training in the Disease mechanisms research group. I would also like to thank my supervisor Aija Kyttälä, for giving me instructions but also for letting me take responsibility of my own work. I am much obliged to the other members of the group and the whole molecular medicine laboratory. I would also like to give special thanks to Markku Lehto and Henna Linturi and would like to acknowledge Nordic Centre of excellence in Disease Genetics and Sigrid Jusélius Foundation. Last but definitely not least, I would like to thank my family and friends for giving me all the support and strength to go forward.

Helsinki, June 2008

University of Jyväskylä
Faculty of Mathematics and Science

Abstract of Master's thesis

Author: Mari Tervaniemi
Title of thesis: Characterization of Neuronal Ceroid Lipofuscinosis Phenotype in Three Different Cell Lines Subjected to RNA interference
Finnish title: Neuronaalisten seroidilipofuskinoosien ilmiasun karakterisointi kolmessa eri RNA hiljennyksellä käsitellyssä solulinjassa
Date: 28.05.2008 **Pages:** 65+2

Department: Department of Biological and Environmental Science
Chair: Molecular biology
Supervisor: Aija Kyttälä

Abstract:

Neuronal ceroid lipofuscinoses (NCL) are a group of genetically inherited encephalopathies, characterized by accumulation of autofluorescent lipopigment in neurons and several other cell types. These diseases are metabolic lysosomal storage disorders affecting mainly children, although some rare adult forms have also been discovered. They are clinically identified by mental and motor deterioration, epileptic seizures, loss of vision and premature death. The disease genotype of NCLs is mainly inherited in an autosomal recessive manner. As an exception, one of the two adult forms (Parry disease) displays dominant inheritance. The different forms of human NCLs are caused by mutations in at least ten genes (CLN1-10), eight of which have been identified (CLN1, CLN2, CLN3, CLN5, CLN6, CLN7, CLN8 and CLN10). Proteins encoded by the NCL genes are mainly located in the lysosomes, late endosomes or the endoplasmic reticulum (ER). These NCL proteins have both soluble and transmembrane forms and thus have various different functions, some of which have been established but most of which are still under research. CLN3 (juvenile NCL, Batten disease) is the most common form of NCL and is enriched especially in the Finnish population. The *CLN3* gene encodes a hydrophobic protein of lysosomal/endosomal membranes, the function of which is still unknown.

The aim of this study was to find an optimal cell line for NCL-targeted RNA interference (RNAi) studies with small interfering RNA (siRNA) transfections, which would show easily detectable markers characteristic of NCL phenotype. In these studies, *CLN3* was chosen as target gene for RNAi and autofluorescent lipopigment accumulation as a NCL marker to be detected. Three cell lines were used for RNAi-experiments and the down-regulation was detected with quantitative real-time PCR. Relatively effective down-regulation of *CLN3* with RNAi was achieved in HEK293 cells, with 70-75% knock-down. The results obtained from HUH7 and SH-SY5Y cells were somewhat controversial, showing unexpected changes also in control-siRNA samples. Accurate down-regulation of *CLN3* was thus not obtained from any of these cell lines, giving a ground for further studies in other cell lines or with different methods. These studies were aiming at laying basis for a larger project, to set up a method that utilizes genome-wide RNAi technology combined with phenotypic screening to detect pathways and genes behind NCL diseases. When succesful, this technology would also create a method for functional studies in human cells, bypassing the use of knock-out mouse models.

Keywords: Encephalopathy, Neuronal ceroid lipofuscinosis (NCL), autofluorescence, lysosomal storage disorder, Batten disease, juvenile NCL (JNCL), CLN3, RNA interference (RNAi), small interfering RNA (siRNA), quantitative real-time PCR (qRT-PCR).

Jyväskylän yliopisto
Matemaattis- luonnontieteellinen tiedekunta

Pro gradu-tutkielman tiivistelmä

Tekijä: Mari Tervaniemi
Tutkielman nimi: Neuronaalisten seroidilipofuskinoosien ilmiasun karakterisointi kolmessa eri RNA-hiljennyksellä käsitellyssä solulinjassa
English title: Characterization of neuronal ceroid lipofuscinosis phenotype in three different cell lines subjected to RNA interference
Päivämäärä: 28.05.2008 **Sivumäärä:** 65+2

Laitos: Bio- ja ympäristötieteiden laitos
Oppiaine: Molekyylibiologia
Tutkielman ohjaaja: Aija Kyttälä

Tiivistelmä:

Neuronaaliset seroidilipofuskinoosit (NCL) ovat ryhmä perinnöllisiä enkefalopatioita eli aivosairauksia, joiden tunnusomaisiin piirteisiin kuuluu autofluoresoivan materiaalin kertyminen hermosoluihin ja moniin muihin solutyyppeihin. NCL-taudit ovat lähinnä lapsuudessa havaittavia lysosomaalisia kertymätauteja, vaikkakin joitakin harvinaisia aikuisiän muotoja on myös löydetty. NCL-tautien kliinisiin piirteisiin kuuluvat henkinen ja motorinen rappeutuminen, epileptiset kohtaukset, näön heikkeneminen ja ennenaikainen kuolema. Ne periytyvät pääasiassa peittyvästi autosomeissa. Poikkeuksena on toinen aikuisiän muodoista (Parryn tauti), joka periytyy vallitsevasti. Näiden aivosairauksien eri muotojen taustalta on löydetty mutaatioita ainakin kymmenessä eri geenissä (CLN1-10), joista kahdeksan on tunnistettu (CLN1, CLN2, CLN3, CLN5, CLN6, CLN7, CLN8 and CLN10). NCL-geenit koodaavat sekä liukoisia proteiineja että kalvoproteiineja, jotka paikantuvat solussa lähinnä lysosomeihin, myöhäisiin endosomeihin ja solulimakalvostoon. Joidenkin NCL-proteiinien tehtävä solussa tunnetaan mutta osa on vielä tutkimuksen kohteina. NCL-taudeista yleisin on CLN3 (juveniili NCL, Battenin tauti), joka kuuluu myös suomalaiseen tautiperintöön. *CLN3*-geeni koodaa hydrofobista lysosomaalista/endosomaalista kalvoproteiinia, jonka varsinainen tehtävä on edelleen selvittämättä.

Tämän tutkimuksen tavoitteena oli löytää optimaalinen solulinja NCL-kohdistettua RNA-hiljentämistä (RNAi) varten pienten häiritsevien RNA molekyyli (siRNA)-transfektioiden avulla. Tarkoituksena oli löytää solulinja, jossa saataisiin helposti esille NCL-ilmiasulle tunnusomaisia merkkejä. *CLN3* valittiin kohdegeeniksi RNAi-testeille ja autofluoresoivan materiaalin keräytyminen tarkasteltavaksi ilmiasupiirteeksi. RNAi-kokeisiin käytettiin kolmea eri solulinjaa (HEK293, HUH7 ja SH-SY5Y) ja vaimennussäätely osoitettiin kvantitatiivisella reaaliaikaisella polymeraasiketjureaktiolla (PCR). Suhteellisen toimiva CLN3:n vaimennussäätely (70-75%) saatiin aikaan HEK293-soluissa. HUH7- ja SH-SY5Y-soluista saadut tulokset olivat ristiriitaisia, johtuen muutoksista myös kontrolli-siRNA-transfektoiduissa näytteissä. *CLN3*:n täydellistä vaimennussäätelyä ei täten saavutettu yhdessäkään valituista solulinjoista, jonka perusteella pääteltiin että jatkotutkimuksissa on käytettävä muita mahdollisia solulinjoja tai menetelmiä. Nämä tutkimukset rakentavat kuitenkin pohjaa laajemmille jatkotutkimuksille, joiden tavoitteena on perustaa teknologia genominlaajuisille RNAi-menetelmille yhdistettynä ilmiasuseulontaan. Näiden menetelmien avulla pystyttäisiin selvittämään reittejä ja geenejä NCL-tautien taustalla. Onnistuessaan tämä teknologia voisi myös luoda vaihtoehtoisen menetelmän toiminnallisille tutkimuksille ihmissoluissa korvaamaan poistogeenisten hiirimallien käytön.

Avainsanat: Enkefalopatia, Neuronaalinen seroidilipofuskinoosi (NCL), autofluoresenssi, lysosomaalinen kertymätauti, Battenin tauti, juveniili NCL (JNCL), CLN3, RNA-hiljennys (RNAi), pieni häiritsevä RNA (siRNA), kvantitatiivinen reaaliaikainen PCR (qRT-PCR).

TABLE OF CONTENTS

ABBREVIATIONS

Ct	Threshold cycle
dsRNA	Double-stranded RNA
GROD	Granular osmiophilic deposit
HEK293	Human embryonic kidney cell line
HUH7	Human hepatoma cell line
JNCL	Juvenile neuronal ceroid lipofuscinosis
miRNA	MicroRNA
NCL	Neuronal ceroid lipofuscinosis
siRNA	Small interfering RNA
q-PCR	Quantitative PCR
GFP-LC3-Ad	Green fluorescent protein-LC3-Adenovirus
qRT-PCR	Quantitative real-time PCR
RT-PCR	Reverse transcription PCR
SAPs	Saposins A and D
SCMAS	Subunit c of mitochondrial ATP synthase
SH-SY5Y	Human neuroblastoma cell line

See appendix 1 for JBC abbreviation standards

INTRODUCTION

1 Encephalopathies

Encephalopathies as a word can be simplified as neurological disorders. They are thus diseases that are caused by the deterioration of variable brain regions leading to multiple disease phenotypes. This deterioration causes alterations in the structure and function of the brain, leading to mental disorders, such as changes in the patient's personality, disturbed concentration, lethargy and progressive loss of memory, consciousness and cognitive ability. Depending on the type of deterioration, neuronal symptoms can also include dementia, seizures, muscular atrophy, myoclonus (compulsive movements), nystagmus (unintentional movement of the eyes), inability to speak or to swallow, visual failure and reduced lifespan. Encephalopathies can be caused by multiple factors, some of them having a genetic basis and some an environmental one. Neurological disorders can thus arise from an infection by bacteria, viruses or prions, or from prolonged exposure to toxic elements, such as solvents, drugs, radiation, paints, industrial chemicals and certain metals. Other causative agents can be metabolic or mitochondrial dysfunction, brain tumors, increased pressure in the skull, chronic progressive trauma, poor nutrition and lack of oxygen or altered blood flow into the brain (http://www.ninds.nih.gov/disorders/encephalopathy/encephalopathy.htm, 11.01.2008).

---

2 Neuronal Ceroid Lipofuscinoses

Neuronal ceroid lipofuscinoses (NCL) are a group of genetically inherited encephalopathies, characterized by accumulation of autofluorescent lipopigment (ceroid lipofuscin) in neurons and many other cell types (Zeman and Dyken, 1969). NCLs are metabolic lysosomal storage disorders, clinically identified by mental and motor deterioration, epileptic seizures, loss of vision and premature death. Although these diseases are considered as the most common

progressive encephalopathies of children, some rare adult forms also exist. The adult forms are characterized by dementia but rarely express blindness. NCLs have also been identified in many other mammalian species, such as dogs, sheep, cats, horses, goats, cattle and mice (for review see Haltia, 2006). The incidence of NCL is up to 1:12 500 live births worldwide, although for some forms of NCLs, the risk is higher in the United States of America and Northern Europe, including Finland (Rider and Rider, 1988; Uvebrant and Hagberg, 1997).

NCLs were presumably first described by a Norwegian physician, Dr. Stengel in 1826 (for review see Haltia, 2006). The first classification into "amaurotic family idiocy" was given by Sachs in 1896, an American neurologist that reported the infantile form of NCLs. Late infantile and juvenile forms were later reported by Batten (1903, 1914) and Vogt (1905, 1907, 1909) in the beginning of the 20th century. During the same time-period, the juvenile NCL was diagnosed also by Spielmayer (1905a, b, 1908) and the late infantile again by Janský (1908) and Bielschowsky (1913). Although NCLs affect mainly children, an adult form was also later reported by Kufs in 1925. The name NCL was proposed by Zeman and Dyken in 1969, based on the ultrastucture of the storage material. NCLs have thus been divided in four main types, depending on the age of onset; infantile NCL (INCL; Santavuori-Haltia disease), late infantile NCL (LINCL; Janský-Bielschowsky disease), variant late infantile NCL (vLINCL; Finnish, Lake-Cavanaugh and Turkish diseases), juvenile NCL (JNCL, Spielmeyer-Vogt-Sjögren disease) and adult NCL (ANCL; Kufs and Parry diseases). Before identification of different genes behind NCLs, the diseases were defined by the age of onset and the ultrastructure of accumulation material.

2.1 Pathology

The pathomorphology of the storage deposits varies between the different forms of NCL. Four distinct ultrastructures have been identified in electron microscopic analyses; fingerprint-like, curvilinear-like, rectilinear-like and granular osmiophilic deposit (GROD) profiles (for review

see Haltia, 2006) presented in Figure 1. The storage bodies have been identified to have a lysosomal origin and are composed mainly of aggregated proteins but also from lipids, carbohydrates and some metals (for review see Seehafer and Pearce, 2006). The main proteinaceous material in these storage bodies has been identified to consist of two types of hydrophobic proteins; subunit c of mitochondrial ATP synthase (SCMAS) or sphingolipid activator proteins A and D (saposins, SAPs) (Palmer et al., 1989; Fearnley et al., 1990; Tyynela et al., 1993). In NCL, the storage deposits are characterized as ceroid lipofuscin. Lipofuscin, or aging pigment, is an accumulative material observed also in normal senescence. The term ceroid is commonly used for a lipofuscin-like accumulation resulting from pathological conditions. The autofluorescent lipopigments appear as yellow/green under ultraviolet (UV) light microscope.

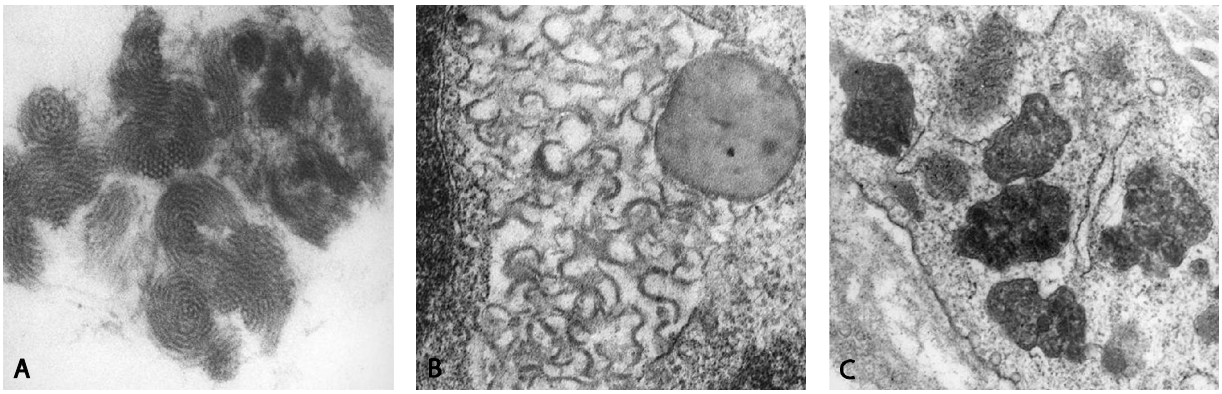

Figure 1: Electron microscope pictures of three types of identified storage deposits in NCL. A: fingerprint-like deposits, **B:** curvilinear- and fingerprint-like deposits and **C:** granular osmiophilic deposits (pictures presented by courtesy of Juhani Rapola).

Massive brain atrophy is one of the hallmarks NCLs. These diseases mainly affect the central nervous system (involving the brain and spinal cord) and cause progressive neuronal loss especially in the cerebral cortex of the brain (Autti et al., 1996). Although accumulation of the storage material has been detected in many cell types, it seems to dramatically disturb only neuronal cells. Magnetic resonance imaging (MRI) experiments of the brain have revealed cerebral and cerebellar deterioration, also observed as a thinner cerebral cortex area. Other

pathological findings are hyperintensity of lobar white matter and hypointensity of thalami (for review see D'Incerti, 2000). The severity of these observations is dependent on the type and onset of the NCL.

2.2 Genetics

Disease genotypes of the NCLs are inherited mainly in an autosomal recessive manner. A rare exception is Parry disease (CLN4B) with autosomal dominant inheritance. The various forms of human NCLs are caused by mutations in different genes. To date, eight of them have been identified and are named as *CLN1* (1p32), *CLN2* (11p15.5), *CLN3* (16p12.1), *CLN5* (13q21.1-32), *CLN6* (15q23), *CLN8* (8pter-p22), *CTSD* (11p15.5) and *MFSD8* (4q28.1-28.2) (The International Batten Disease Consortium, 1995; Vesa et al., 1995; Sleat et al., 1997; Savukoski et al., 1998; Ranta et al., 1999; Gao et al., 2002; Wheeler et al., 2002; Siintola et al., 2006, 2007; Steinfeld et al., 2006). The genes for CLN4 and CLN9 are yet to be identified. There have also been implications that deficiencies in the genes for certain cysteine proteases (cathepsins B, L and F) (Felbor et al., 2002; Koike et al., 2005; Tang et al., 2006) and chloride channels (ClC-3 and -7) cause pathological symptoms similar to the NCLs (Yoshikawa et al., 2002; Kasper et al., 2005). The mutations identified in the different genes are listed in a NCL mutation database: http://www.ucl.ac.uk/ncl/. Separately these diseases are thus monogenic but the heterogeneity in their origin, together with the similarity of a common phenotype and clinical symptoms, classifies them as a fine model for complex diseases.

2.3 NCL proteins and specific features

Proteins encoded by the NCL genes are mainly located in the lysosomes, late endosomes or the endoplasmic reticulum (ER). The NCL proteins have both soluble and transmembrane forms (for review see Kyttälä et al., 2006) and thus have various functions, some of which have been established but most of which are still under research. The diversity of the genes

encoding NCL proteins suggests a common or related pathway underlying the the similar phenotypes of the different NCL-subtypes, which are also referred to with the abbreviation CLN (ceroid lipofuscinosis, neuronal).

NCL expressing the infantile age of onset (INCL) causes the most severe form of these diseases and is especially abundant in the Finnish population (Vesa et al., 1995). INCL is caused by mutations in the *CLN1* gene, which codes for a soluble enzyme, palmitoyl-protease thioesterase (PPT1) (Camp et al., 1994; Vesa et al., 1995). Palmitoyl-protease thioesterase is an enzyme that removes palmitate groups from lipid-modified proteins. In non-neuronal cells this enzyme is mainly located in the lysosomes (Vesa et al., 1995; Verkruyse and Hofmann, 1996) but in mature neurons it is also found in synaptosomes and synaptic vesicles at the axonal presynaptic area (Heinonen et al., 2000; Lehtovirta et al., 2001; Ahtiainen et al., 2003). The ultrastructural profile of infantile NCL is characterized by the granular osmiophilic deposit morphology, including saposins A and D as the major components of the storage material (Tyynelä et al., 1993). Except for the classical infantile onset of these diseases, some mutations of *CLN1* can cause disease phenotypes with late-infantile, juvenile or adult age of onset (Becker et al., 1979; Hofman and Taschner, 1995; Philippart et al., 1995; Das et al., 1998; van Diggelen et al., 2001).

The gene *CLN2* also codes for a soluble lysosomal enzyme, which underlies the classical form of late infantile NCL (LINCL) (Rawlings and Barrett, 1999). The CLN2 protein; tripeptidyl peptidase (TPP1) is a member of serine carboxyl proteinase family, functioning as an enzyme that removes tripeptides from the N-terminal ends of some small proteins such as subunit c of mitochondrial ATP synthase (Wlodawer et al., 2001). Ultrastructures with curvilinear bodies have been considered as the hallmark of CLN2. However, some mutations causing a later age of onset may also contain fingerprint and granular osmiophilic deposit structures (Wisniewski et al., 1999).

All the other NCLs with late infantile onset have been divided in many variant subtypes (vLINCL) that are caused by mutations in different genes. These variant types are frequently

connected to different founder populations. CLN5 is often referred to as Finnish late variant NCL, according to the abundance of this disease type especially in Finnish NCL patients. Some NCLs outside of Finland with *CLN5* mutation have been also found to represent a juvenile onset (Pineda-Trujillo et al., 2005). The *CLN5* gene has been suggested to encode both soluble and transmembrane forms of a lysosomal glycoprotein with still unknown function (Savukoski et al., 1998; Vesa et al., 2002). The ultrastructures of storage bodies mainly represent fingerprint and curvilinear profiles (Santavuori et al., 1982; Tyynela et al., 1997). Portuguese/Costa Rican variant late or early juvenile type of NCL is caused by mutations in the *CLN6* gene. This gene codes for a transmembrane protein with seven membrane spanning domains, localized to the endoplasmic reticulum (ER) (Gao et al., 2002; Heine et al., 2007). The ultrastructural profiles of CLN6 represent granular, curvilinear and fingerprint profiles (Lake and Cavanagh, 1978; Andermann et al., 1988; Elleder et al., 1997). This sort of profiles are also present in CLN7 and CLN8, of which CLN7 has a variant late infantile age of onset represented especially in Turkish patients (for review see Mole et al., 2005). CLN7 has been recently identified to be caused by mutations in the *MFSD8* gene, coding for a putative transporter protein of lysosomal membranes, with twelve predicted transmembrane domains (Siintola et al., 2007). CLN8 has been recognized to have two clinically different late-infantile variant phenotypes; Turkish/Mediterranean (Ranta et al., 2004; Zelnik et al., 2007) and Finnish (Northern epilepsy; an allelic variant of *CLN8*) (Ranta et al., 1999; Herva et al., 2000). *CLN8* codes for a transmembrane protein, localized to ER and partially to ER-Golgi intermediate compartment (ERGIC) in non-neuronal cells (Lonka et al., 2000). In polarized cells (such as neuronal cells) these proteins have been suggested to reside also in other organelles outside the ER (Lonka et al., 2004). Function of this protein is not known but it is proposed to be a member of TRAM-LAG1-CLN8 (TLC) protein family (a protein family possessing a TLC domain and connected to multiple functions such as lipid trafficking, metabolism, or sensing) (Winter and Ponting, 2002). The main component in all late-infantile NCL storage bodies is mitochondrial ATP synthase subunit c (Jolly et al., 1989; Palmer et al., 1992; Tyynela et al., 1997; Topcu et al., 2004; Koike et al., 2005).

The classical juvenile NCL (JNCL) has been defined by mutations in *CLN3* gene, encoding a transmembrane protein with six membrane spanning domains (Janes et al., 1996; Kyttälä et al., 2004). CLN3 is the most common form of NCLs worldwide and therefore probably the most extensively studied. Many roles have been proposed but the main function of this protein has remained elusive. Lipopigments of CLN3 represent fingerprint profiles (for review see Santavuori, 1988), containing mitochondrial ATP synthase subunit c as the major storage component (for review see Kominami et al., 1995). JNCL (often called as Batten disease) and the CLN3 protein are discussed in more detail in Chapter 3. A variant form of juvenile NCL (vJNCL) has also been reported (Schulz et al., 2004) and named CLN9. It is caused by a yet unidentified gene but the protein is proposed to function as a regulator of dihydroceramide synthase (Schulz et al., 2006).

The rare adult forms of NCL have neither yet been identified. They are divided into two groups, of which the CLN4A (Kufs' disease) has an autosomal recessive inheritance common for NCLs, while CLN4B (Parry disease) is different in perspective to inheritance and thus expresses an autosomal dominant form of heritability (Ferrer et al., 1980). CLN4s display a combination of granular, curvilinear and fingerprint patterns (for review see Mole et al., 2005), containing mitochondrial ATP synthase subunit c or saposins A and D as storage material (Sadzot et al., 2000; Nijssen et al., 2003).

A congenital form of NCL has also been reported (Barohn et al., 1992). It is named CLN10 but is caused by mutations in the gene *CTSD* (Siintola et al., 2006; Steinfeld et al., 2006). This gene codes for cathepsin D, a soluble lysosomal aspartic protease (Dean, 1975; Tang and Wong, 1987). The storage deposits show accumulation of saposins A and D (Tyynelä et al., 1993) and mitochondrial ATP synthase subunit c (Koike et al., 2005). Some of the features of NCLs described in this chapter are collected together in Table 1. All of the NCLs show similarity in pathology and biochemistry, including interactions between different NCL proteins and protein compartments (Vesa et al., 2002; Persaud-Sawin et al., 2007). According

to these findings, it has been suggested that the NCL proteins reside in a common metabolic pathway.

Table 1 Neuronal ceroid lipofuscinoses; classification and function.

Disease	Gene	Protein	Locus	Location	Topology	Main storage material
CLN1	*CLN1*	PPT1	1p32	Lysosomes, synaptosomes, synaptic vesicles	Soluble/ membrane associated	SAPs
CLN2	*CLN2*	TTP1	11p15.5	Lysosomes	Soluble	SCMAS
CLN3	*CLN3*	CLN3/ Battenin	16p12.1	Lysosomes, Endosomes, Cell membrane, Synaptosomes	Transmembrane	SCMAS
CLN4 A and B	?	CLN4	?	?	?	SCMAS, SAPs
CLN5	*CLN5*	CLN5	13q21.2-32	Lysosomes	Soluble	SCMAS
CLN6	*CLN6*	CLN6	15q21-23	ER	Transmembrane	SCMAS
CLN7	*MFSD8*	MFSD8	4q28.1-28.2	Lysosomes	Transmembrane	SCMAS
CLN8	*CLN8*	CLN8	8pter-p22	ER, ERGIC	Transmembrane	SCMAS
CLN9	?	CLN9	?	?	?	?
CLN10	*CTSD*	Cathepsin D	11p15.5	Lysosomes	Soluble	SAPs, SCMAS

Abbreviations: SAPs; saposins A and D, SCMAS; subunit c of mitochondrial ATP synthase, PPT1; palmitoyl-protease thioesterase, TPP1; lysosomal enzyme tripeptidyl peptidase, ER; endoplasmic reticulum, ERGIC; ER-Golgi intermediate compartment.

3 Batten Disease (JNCL) and the CLN3 protein

CLN3 (JNCL, Batten disease) has the incidence of 1:21 000 live births and is enriched especially in the Finnish population (Mitchison et al., 1995). JNCL is most commonly caused by a 1.02-kb deletion of exons 7-8 at the *CLN3* gene, resulting in a frameshift after the 153rd amino acid residue and leading into production of a truncated protein (The International Batten Disease Consortium, 1995). The mutant protein has been presumed to remain non-functional but recent studies have suggested a function regulating lysosomal size (Kitzmuller et al., 2008). The CLN3 protein (Battenin) contains 438 amino acids but has also several splice variants (Cotman et al., 2002; Narayan et al., 2004). It is produced as a single ~43kDa

precursor, which is N-glycosylated at the ER membrane and then targeted to lysosomes via two targeting motifs (Järvelä et al., 1998; Kyttälä et al., 2004). The CLN3 protein has thus been localized mainly to lysosomes and endosomes (Järvelä et al., 1998; Kyttälä et al., 2004), but has also been reported to localize at the cell membrane (Margraf et al., 1999). In neuronal cells, the CLN3 protein resides in the synaptosomes but is not targeted to the synaptic vesicles (Luiro et al., 2001). In these detergent-resistant membranes the protein has been reported to co-localize with lipid rafts (Rakheja et al., 2004) and has been reported to contain a galactosylceramide (GalCer) lipid raft-binding domain (Persaud-Sawin et al., 2004). The coding sequence of this domain is deleted in the disease gene with the most common mutation.

Although the precise function of the CLN3 protein is not known, it has been reported to exhibit a novel palmitoyl-protein Δ-9 desaturase activity (Narayan et al., 2006). The protein has been also suggested to take part in lysosomal pH homeostasis, import of arginine into lysosomes, cytoskeletal function involved in membrane trafficking, synthesis of the phospholipid bis(monoaglycerol)phosphate, and regulation of ceramide generation connected to apoptosis and cell growth, possibly via the previously mentioned galactosylceramide lipid raft-binding domain (Pearce and Sherman, 1998, 1999; Pearce et al., 1999; Persaud-Sawin et al., 2002, 2004; Kim et al., 2003; Luiro et al., 2004, 2006; Hobert and Dawson, 2007). One of the functions suggested for CLN3 has been connected to the maturation of autophagosomes (Cao et al., 2006). Autophagy is a process involved in the turnover of cytoplasmic components, such as mitochondria (for review see Cuervo, 2004). Autophagy is thus involved in the normal housekeeping of the cells but is also induced and initiated by response to stress or starvation. The process begins by the engulfment of target elements, leading into acidification and maturation of the autophagosomes into autolysosomes by fusion with late endosomes or lysosomes. Studies with homozygous *Cln3*$^{\Delta Ex7/8}$ mice have shown an increase in autophagosome formation but deficiency in autophagosome maturation into autolysosomes (Cao et al., 2006).

4 RNA Interference

Messenger RNAs (mRNA) function as a link between the genes and the proteins. The information included in the DNA is delivered by the mRNAs to the translation machineries, which then use this information to synthesize proteins. This makes mRNA a suitable target for inhibition of protein synthesis and thus gene expression silencing without altering the DNA. RNA interference (RNAi) is a highly conserved defense mechanism by which expression of specific genes can be inhibited post-transcriptionally. It is triggered by RNA molecules that have double-stranded structures and is based on a sequence specific nucleolytic destruction of target mRNA or inhibition of protein translation by other means.

4.1 Naturally occurring RNAi

RNAs have been found to have many regulatory roles, beside the familiar ones as messenger RNAs (mRNA), transfer RNAs (tRNA) and ribosomal RNAs (rRNA). One of the less familiar regulatory mechanisms is RNAi, which was discovered through three independent findings. Gene silencing was first identified in plants and fungi, where it was induced by expression of viral replication (for review see Baulcombe, 2004). Mello and Fire (1998) discovered that introducing both sense and antisense RNA as dsRNA could result in potent, specific and long lasting gene expression silencing in nematode *Caenorhabditis elegans.* They also received the Nobel Prize in Physiology or Medicine in 2006, based on these discoveries. MicroRNAs (miRNA) were first discovered by Ruvkun and Ambros, who studied the developmental timing genes, also in *Caenorhabditis elegans.* They found a gene (*lin4*) coding for two miRNAs, also defined as small temporal RNAs (stRNA) (Lee et al., 1993; Wightman et al., 1993).

miRNAs are naturally occurring inducers of RNAi and possess the same machineries for gene expression inhibition as RNAi with exogenously introduced components. Instead of destroying the mRNA, miRNAs only inhibit protein translation by annealing with the

3´untranslated region of the target mRNA (Lee et al., 1993; Reinhart et al., 2000). They are small single-stranded RNA (ssRNA) molecules that are produced as about 70- nucleotide long precursors. The molecule contains an inverted repeat, which forms a hairpin-like double-stranded secondary structure with bulges and loops. miRNAs have been found to have regulatory roles in the developmental programs of several organisms and many of them have also been found in humans and mice (Lagos-Quintana et al., 2001; 2002; Mourelatos et al., 2002). RNAi has also been considered to have a role in defense against nucleic acid invaders such as viruses, transposons and transgenes, acting as a nucleic acid immune system (Gitlin et al., 2002; Sijen and Plasterk, 2003). In response to nucleic acid invaders the mechanism of interference cleaves the foreign genome into dsRNAs which trigger RNAi against the mRNAs of the invader.

4.2 Experimental RNAi

The experimental RNAi is caused by introduction of exogenous double-stranded RNAs into the cells. In this process, the dsRNAs (preferably without any bulges and loops) are transfected or injected into the cell cytoplasm. These foreign RNA molecules trigger the RNAi pathway, by which the dsRNAs are processed into smaller, 21- 23-nucleotide long small interfering RNAs (siRNA) with 2-nucleotide overhangs at their 3’ ends (see enlargement of siRNA structure in Figure 2). Although longer dsRNA can be used to induce RNAi in most animal cells and embryonic cells of mammals, in most adult mammalian cells the system is different. In these cells, the long dsRNA turns on the interferon response (for review see Stark et al., 1998) which is a primitive antiviral mechanism that activates general degradation of mRNA, thus down-regulating the protein synthesis and eventually leading into apoptosis. Elbashir et al. discovered in year 2001 that RNAi can be used also in mammalian cells, by utilizing 21-nucleotide long siRNA with liposome transfection. The short sequence of these RNA molecules enables them to bypass the interferon system, which detects only longer RNA molecules as invaders. Introducing exogenous dsRNAs or siRNAs for induction of RNAi will

result in fairly long lasting but transient silencing of targeted genes. Sustained silencing can be achieved with transgenes, such as vectors that express exogenous short hairpin RNA (shRNA) precursors, in the same way as miRNAs in natural systems (Brummelkamp et al., 2002; Paddison et al., 2002).

4.3 Mechanism for gene expression silencing via RNA interference

The RNAi pathway is initiated by the processing of double stranded RNA molecules into smaller fragments; siRNAs or miRNAs. In the case of endogenous miRNAs, the ~70 nucleotide precursor molecule is first cleaved with two different double-strand specific ribonucleases; drosha and dicer (type III "dicers"). The first cleavage is performed in the nucleus by drosha, which acts at the end of the hairpin structure, producing a dsRNA molecule with bulges and loops. In the following step, these modified RNA molecules are exported to the cytoplasm by Exportin-5 to be cleaved further by Dicer, resulting in the production of 21-23 nucleotide long mature miRNAs (for review see Ambros, 2001; Hammond, 2005).

siRNAs result from the Dicer-mediated cleavage of dsRNAs derived from digested nucleic acid invaders or exogenous dsRNAs experimentally introduced into the cells. If the experimental siRNA is produced via stable expression and production of short hairpin RNA precursors in the nucleus, they are processed and exported into the cytoplasm with a similar method described earlier for miRNAs. The two strands of the siRNA duplexes are separated by a helicase in the cytoplasm and the guide strand (see Figure 2) of the siRNA is connected with several other components in siRNA containing ribonucleoprotein complex (siRNP), which is now called as RNA-induced silencing complex (RISC) (Nykänen et al., 2001). The guide strand is assembled into the RISC in an end-specific manner that includes recognition of the 5´- phosphate and the seed region (bases 2 to 8 on guide strand, see Figure 2) by argonaute ("slicer"), which is a ribonuclease H enzyme included in the RISC. The first nucleotide does not base pair with the target mRNA, instead it is bound by a pocket in the argonaute. The

binding efficiency into the argonaute is also controlled by the strength of 5´end binding of the guide strand to the passenger strand, which should be weak (preferably beginning with A or U). The RISC complex guides siRNA for complementary base pair binding to the target mRNA, which is cleaved by the argonaute after recognition of exact complementarity. miRNAs function via a similar pathway as siRNAs described here, but do not result in the digestion of the target. Some siRNAs do not induce cleavage either, if there are mismatches between the siRNA and the target mRNA. The presence of the RISC will still inhibit translation. Even though miRNAs and siRNAs share the core machinery for RNAi, some exceptions have been found in the preference of RISC components, such as different forms of argonaute enzymes (Okamura et al., 2004).

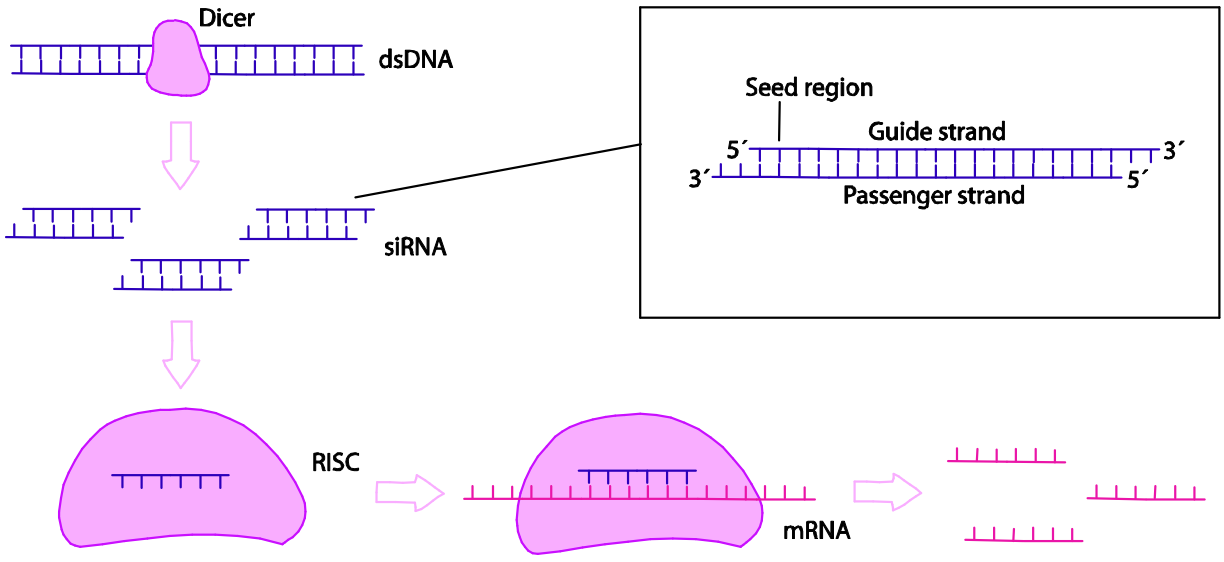

Figure 2: Basic mechanism of RNA interference. In this process, the dsRNA is first cut by Dicer into siRNAs, of which a more accurate description is shown in the magnification box. The guide strand of the siRNAs are assembled with several other components to form a RNA-induced silencing complex (RISC), which further guides the binding of siRNA to the target mRNA. The target is cut into pieces by Argonaute enzyme included in the RISC. Figure modified from (Mocellin and Provenzano, 2004).

4.4 Problems in RNAi-mediated gene silencing

Introduction of exogenous nucleic acids can cause changes in gene expression or in the phenotype of the cell. Effects caused for example by transfections, injections or by the foreign nucleic acid itself can be controlled by a non-specific or scrambled RNAi construct. This is especially useful when using quantification of gene expression, in which case any side-effects can be ruled out or taken into account. The main problems observed in RNAi-experiments especially in mammalian systems, are off-target effects, induction of innate immune system and saturation of RNAi machinery. Off-target effects are caused by non-specific binding of RISC to a wrong target, allowed by mismatches along the sequence outside the seed region of the guide strand siRNA (see Figure 2) (Jackson et al., 2003). The occurrence of off-targeting is not easy to detect but can be avoided (Echeverri et al., 2006). The methods to achieve reliable results include redundancy and rescue, preferably with multiple scrambled or non-targeting controls. Redundancy in this association means utilization of at least two different siRNAs, directed separately on the same target. Rescue involves experiments involving restoration of the original situation in affected cells (allowing gene expression or introducing the inhibited product).

Non-specific induction of innate immune system can be caused by several reasons, such as the concentration and structure of the siRNA or via interferons (IFN) or toll-like receptors (TLR), as reported in several experiments (Semizarov et al., 2003; Sledz et al., 2003; Kariko et al., 2004; Gondai et al., 2008). Saturation of RNAi machinery occur upon over-expression of stably expressed siRNAs or by introduction of exogenous siRNAs in excess (Barik, 2006). Introducing two distinct siRNAs simultaneously can lead to competitive inhibition, specified by the 5´-end of the guide strand siRNA (Yoo et al., 2008). This inhibition can thus restrain the gene silencing of one of the introduced siRNAs.

5 Quantitative real-time PCR

Quantitative PCR (qPCR) is a method that enables amplification of specified DNA molecules and estimation of their number in a sample. This estimation can be used when comparing the quantity of DNA in separate samples or even the amounts of different DNAs in the same sample, giving a relative value of difference between them. The amount of PCR end-point products can be easily detected by agarose gel electrophoresis. The resolution is fairly poor in this method, requiring high fold changes in the samples; only a minimum of 10-fold changes can be detected. Probably the most sensitive method of measuring the target DNA amplification is real-time PCR. With this method, the quantity of DNA is analyzed in real time after each PCR cycle, resulting in the detection of even minimal changes. This method also enables the detection of DNA at the exponential phase of the PCR, giving accurate values for quantification. Real-time PCR has many applications, such as genotyping, viral quantification, expression microarray data verification, drug therapy efficacy, DNA damage measurement, pathogen detection, as well as assay verification and validation (Ginzinger et al., 2000; Lander et al., 2001; Nigro et al., 2001; Venter et al., 2001; Cai et al., 2005; Shannon et al., 2007). Here, the main focus will be on gene expression quantification (for review see Lockhart and Winzeler, 2000).

5.1 Mechanism of quantitative real-time PCR

Quantitative real-time PCR (qRT-PCR) method uses fluorescent markers for obtaining information about amplification. There are two methods available, utilizing either fluorescent double-stranded DNA dyes or fluorescent reporter probes.

Double-strand DNA dyes. These dyes, such as SYBR Green (Schneeberger et al., 1995), bind non-selectively to all double-stranded DNAs (see Figure 3A). Unfortunately they also bind the primer dimers, resulting in fluorescence from all of the double stranded DNA molecules

available. SYBR Green dye binds to the minor groove of the double-strand, resulting in an emission of fluorescence, which increases when the target amplification progresses.

Reporter probes. Fluorescent reporter probes are more accurate in detecting target amplification; the probe is sequence specific and will only bind the specified target cDNA (see Figure 3B). This method also enables the use of multiple probes labelled with different colours. Different probes can thus bind different targets in the same sample. The probe usually contains a fluorescent reporter at one end and a quencher, repressing reporter fluorescence, at the other end. Exonuclease activity of the PCR DNA polymerase cuts down the probe, removing quencher and allowing the reporter to fluoresce. TaqMan probes (Heid et al., 1996) and primers used with Taq polymerase are most commonly used for fluorescence detection.

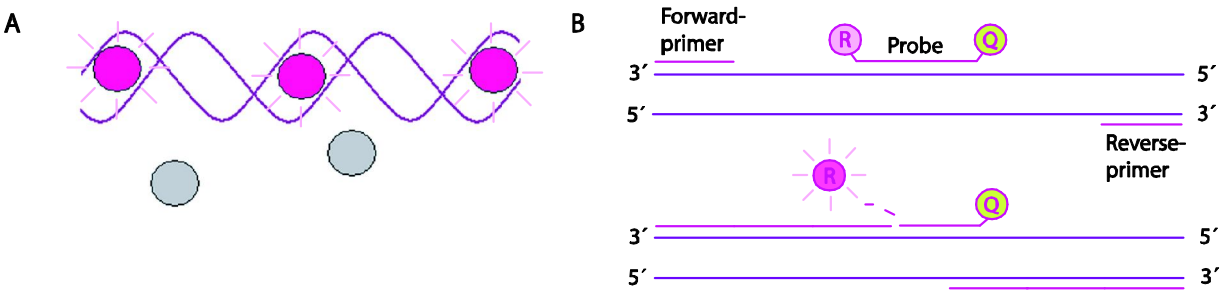

Figure 3: The two methods for quantitative real-time PCR. A: Double-strand DNA dyes, such as SYBR Green bind to the double-stranded DNA. Fluorescence increases as the target DNA is being amplified. **B:** Reporter probes bind in a sequence-specific manner to the target strand. As the complementary strands are synthesized, they dislocate the probes, which are cut into pieces. The reporter (R) and quencher (Q) lose their interconnection and the reporter molecule is now free to fluoresce. Figure modified from Real-time PCR versus traditional PCR instructions provided by Applied Biosystems.

5.2 Expression level quantification

Expression level quantification via mRNA (Delidow et al., 1989) involves a two-stepped PCR. In the first reaction, cDNA is produced by reverse transcription PCR (RT-PCR) from the extracted total RNA, using either random primers or oligo dT primers. This reaction synthesizes a single stranded DNA complementary to the coding strand RNA. The second

strand is produced in the second step by using specific primers that are targeted on the cDNA representing the gene whose expression is being analyzed. The first cycle of the PCR reaction synthesizes a second strand only for the specific cDNA and the following cycles amplify these double stranded cDNAs leading to exponential scale of amplification, depending on the efficiency of the PCR reaction. A 100% efficiency of a PCR reaction requires doubling of every PCR amplicon during the geometric phase of the PCR amplification.

Real-time PCR efficiency can be analysed from a standard curve. This experiment involves dilution series with known cDNA concentrations, represented graphically as a semi-logarithmic regression line plot of the Ct values versus the logarithmic input of nucleic acids. The slope indicates the efficiency of reaction, -3.32 representing 100% efficiency (Pfaffl, 2001). More negative slope values indicate less efficient PCR reactions. More positive values can be caused by low quality samples or problems in pipetting. The percentage of efficiency (E) can be calculated with Equation 1:

$$E = (10^{-1/\,slope} - 1) \times 100 \qquad \mathbf{1}$$

Relative quantification of gene expression involves analysis of at least two different genes: target, which is the gene of interest (or genes if multiple targets are analyzed), and an endogenous reference gene (positive control of the reaction), against which the target gene expression is normalized (Freeman et al., 1999). An endogenous control is usually a stably expressed housekeeping gene such as 18S rRNA, GAPDH or β-actin.

5.3 Analyzing the expression differences

There are several methods available for analyzing results of gene expression quantification and the choise of a suitable method depends on various factors (Bookout et al., 2006). In the experiments of this master's thesis, products and applications provided by Applied Biosystems have been used. Applied Biosystems supports two methodologies for relative quantification of

gene expression; Relative Standard Curve Method and Comparative Turnover Cycle (Ct) Method (ΔΔCt) (Tsai and Wiltbank, 1996; Livak and Schmittgen, 2001).

Relative Standard Curve Method. In this approach, the PCR efficiencies of the target and endogenous control do not need to have an equivalent slope value. Less amount of validation is thus needed for the reaction setup. Precise values for quantification can be acquired since the method is based on interpolating results from the standard curves. According to this, every plate should contain samples for standard curves, requiring more reagents and space in the experiments. This method is thus suitable for experiments involving few samples and targets.

Comparative Ct Method. This method does not require standard curve setup on every plate and is especially useful when using the TaqMan detection system (in which the amplification is guaranteed to have 100% efficiency). This approach is useful when using high numbers of targets and samples. It may also be considered for high throughput systems microarray validations. This method uses an arithmetic formula for data analysis, which is shown in Equation 2 (and used in the data analysis of the q-PCR results in this master's thesis):

$$2^{-\Delta\Delta Ct} \qquad \textbf{2}$$

Other methods have also been presented, concentrating on the same principles as described above but focusing on different factors in the experiments. One of the examples is focused on real-time PCR efficiencies (efficiency-corrected ΔCt method) and the crossing point deviation between an unknown sample and a control (Pfaffl, 2001). Quantification can be calculated using of Equation 3:

$$Ratio(R) = \frac{(E_{t\arg et})^{\Delta Ct_{t\arg et}(sample-control)}}{(E_{t\arg et})^{\Delta Ct_{t\arg et}(sample-control)}} \qquad \textbf{3}$$

AIM OF THE STUDY

The aim of this study was to find an optimal cell line for RNAi studies targeted on NCL genes. The optimal cell line expressing functional RNAi would represent some phenotypic NCL markers that would be easily detected by immunofluorescence. These studies serve as a pilot experiment for a larger project, aiming at setting up a method that utilizes genome-wide RNAi technology combined with phenotypic screening to detect pathways and genes behind genetic diseases. When succeeded, this technology would also create a method for functional studies in human cells, bypassing the use of knock-out mouse models.

The work can be divided in three main tasks:

1. Down-regulation of *CLN3* with RNAi in HEK293, HUH7 and SH-SY5Y cells.

2. Measurement of the *CLN3* knock-down efficiency with quantitative PCR and detection of the appearance of NCL markers with immunofluorescence studies.

3. Testing of RNAi-treated cells for functional studies.

MATERIALS AND METHODS

1 Cell lines

RNAi experiments were performed in three human cell lines; HEK293 (human embryonic kidney cell line), HUH7 (human hepatoma cell line) and SH-SY5Y (human neuroblastoma cell line). HEK293 and HUH7 cells were acquired from Vesa Olkkonen (Department of Molecular Medicine, National Public Health Institute and Institute for Molecular Medicine Finland, Finland). The HEK293 cells were maintained in Dulbecco's modified Eagle's medium (DMEM, Sigma) and the HUH7 cells in Eagle Minimum Essential Medium (Eagle MEM, Sigma), both supplemented with 10% fetal calf serum (FCS), 50 mg/ml streptomycin and 100 IU/ml penicillin. Both cell lines were split twice a week, HEK293 1:4 and HUH7 1:3. SH-SY5Y cells were provided by Folkhälsan Institute of Genetics (Department of Medical Genetics, Finland) and maintained in 1:1 DMEM and Ham´s F12 medium (Sigma), supplemented with 10% fetal calf serum (FCS), 50 mg/ml streptomycin, 100 IU/ml penicillin and first with 10mM 4-(2-hydroxyethyl)-1-piperazineethanesulfonic acid (HEPES), which was later excluded, but 0,1% non-essential amino acids (NEAA) was added. SH-SY5Y cells were split 1:5 once a week when maintained in a medium sized flask. Two types of fibroblasts were used for phenotyping studies; mouse embryonic wild type fibroblasts as a control and mouse embryonic knock-out *Cln3* skin fibroblasts (Mitchison et al., 1999) for autofluorescence accumulation studies. These cells were maintained in DMEM supplemented with 20% fetal calf serum (FCS), 50 mg/ml streptomycin and 100 IU/ml penicillin.

2 siRNA transfections

siRNA transfections were used to silence *CLN3* expression. Two different siRNAs targeting exons 6 and 10 with the following sequences: siRNA-Ex6; 5´-

GUGGGAUUUGUGCUGCUGGAA-3´ and siRNA-Ex10; 5´-CCAGCCUCUCCCUUCGGGAAATT-3´ were used simultaneously in RNAi studies. siRNA duplexes were ordered from Sigma-Proligo.

The cells used later for q-PCR analysis were seeded in 9.6cm^2 wells one day before transfection. Transfection optimization was first carried out with a fluorescent CTRL-F control-siRNA (Sigma-Proligo) and later with BLOCK-iT Fluorescent Oligo control-siRNA (Invitrogen). Transfection efficiency was optimized close to 90%, as detected with confocal microscope. HEK293 cells were seeded 4×10^5 cells per well (covered with 0.4% gelatin [Sigma]) and transfected once with 500pmol of both siRNAs, using 10µl Lipofectamine^{TM} 2000 transfection reagent (Invitrogen). HUH7 cells were seeded at 5×10^5 cells per well and transfected twice with 340pmol of both siRNAs, also using 10µl Lipofectamine^{TM} 2000. The second transfection was performed 48 hours after the first transfection. The cells were detached and seeded again between the transfections. SH-SY5Y cells were seeded 2×10^6 cells per well (covered with 0.4% gelatin [Sigma]) and transfected twice with 500pmol of both siRNAs by using 9µl Lipofectamine^{TM} 2000. The second transfection was performend 48 hours later. The cells used for immunofluorescence analyzes were grown in 1.9cm^2 wells and transfected with the same concentrations of siRNAs and Lipofectamine^{TM} 2000. A non-specific control siRNA: siCONTROL Non-Targeting siRNA #1 (Dharmacon, Thermo Fisher Scientific) was transfected to control for non-specific effects caused by the transfections.

3 RNA extraction and cDNA synthesis

Total RNA was extracted from HEK293, HUH7 and SH-SY5Y cells plated on 6-well plates, at two, four and six days after the first transfection. RNeasy Mini Kit (Qiagen) was used for the isolation with Heraeus Biofuge Pico (DJB labcare) tabletop centrifuge. Concentration and purity of the isolated RNA was measured with NanoDrop® ND-1000 Spectrophotometer (NanoDrop Technologies, LLC, Thermo Fisher Scientific) and the possible fragmentation of

the RNA was tested from HUH7 cell samples transfected with CLN3-siRNA on Day 2, Day 4 and Day 6 with Bioanalyzer (Agilent Technologies). The extracted RNAs were stored in -70°C between the experiments. DNA contamination was not considered to be relevant in these experiments, because the primers to be used later in qRT-PCR were designed on exon-exon boundaries. The sequences in the RNAs were converted into cDNA via reverse transcription. cDNA synthesis of the RNA extracted from HEK293 cells was performed with Advantage RT-for-PCR Kit (Clontech) by using 1µg of total RNA and oligo dT primers, according to the manufacturer's instructions. RT-PCR for q-PCR Kit (Dynamo) was used for the cDNA synthesis for RNA originating from the HUH7 and SH-SY5Y cell extracts; also with 1µg total RNA and with oligo dT primers, according to manufacturer's instructions. cDNAs were diluted with RNase free Molecular biology grade water (Eppendorf) (diethylpyrocarbonate [DEPC] water was not considered suitable for the following real-time PCR reactions, due to the manufacturer's recommendation).

4 Quantitative PCR

Q-PCR was used to observe the knock-down of *CLN3* expression. The knock-down of *CLN3* was first analyzed with the End-point PCR method. This method was modified to represent not only the final amount of amplified product but also the amounts at the exponential phase of amplification. This was performed by taking samples at different points of the PCR cycles (10, 16, 22, 28, end point; 34). Different dilution series were also produced from the cDNA; 1:1, 1:10, 1:15 and 1:20. 20 µM CLN3-Y2H-2F (5´-ACTGAATTCACATCTCCTGAGGCCCAGG-3´) and CLN3-Y2H-2R (5´-GTCGGATCCACCCTTGAATACTGTCCACCT-3´) primers (Genset oligos, Sigma-Proligo) were used for the PCR with 0.02U/µl Dynazyme II (Finnzymes) performed in DNA Engine Dyad^{TM}-Peltier Thermal Cycler (MJ Research). The PCR products were analyzed by electrophoresis on 1.5% agarose gels (GellyPhor, Euroclone) stained with SYBR Safe^{TM} DNA Gel Stain (Invitrogen), and the size of the bands compared to a 50bp ladder size marker

(Fermentas). This method did not produce results that could be used for accurate quantification.

In order to achieve quantitable results, real-time PCR was performed with ABI PRISM 7000 Sequence Detection System (Applied Biosystems, Folkhälsan Institute of Genetics, Folkhälsan Research Center, Helsinki, Finland) by using pre-designed TaqMan® Gene expression Assay primers and probes (Applied Biosystems) for *CLN3* (Hs00164002_m1) and for an endogenous control, the gene encoding TATA binding protein; *TBP* (Hs99999910_m1). MicroAmp™ Optical 96-Well Reaction Plates with Barcode, MicroAmp™ Optical Adhesive Films and TaqMan® Univermal PCR Master Mix were also from Applied Biosystems. Standard curves were first made for all the three cell lines. Samples were run in triplicates of 25µl for each reaction, including 2× master mix (12.5µl), 20× TaqMan assay oligomer (1.25µl), H_2O and cDNA. For the actual run, 200ng of HEK293 cDNA per sample (measured with NanoDrop) was used. The cDNA concentrations were not measured for HUH7 and SH-SY5Y cells. Instead, for these cell line studies, 5µl of cDNA was used for each reaction. The following protocol for the sequence detection system was performed: uracil-N-glycosylase (UNG) activation 50°C for 2 min, denaturation at 95°C for 10 min, amplification cycles repeated 50 times, 95°C (denaturation) for 15 sec and annealing/extention at 60°C for 1 min, detection of fluorescence in the end of each cycle. The data was analyzed with the ΔΔCt method by normalizing the relative expression of *CLN3* for the expression of *TBP*.

5 Immunofluorescence analysis

siRNA-transfected cells seeded on coverslips were fixed with 4% paraformaldehyde (PFA) in phosphate buffer saline (PBS), permeabilized with 0.2% saponin and immunostained for phenotyping assays. HEK293 and HUH7 cells were labeled with subunit c rabbit antiserum (1:1000 or 1:500) (Palmer et al., 1995) provided by Jaana Tyynelä-Vesterinen (Institute of Biomedicine/Biochemistry and Neuroscience Research Program, Biomedicum Helsinki,

University of Helsinki) followed by Rhodamine-Red-X conjugated goat anti-rabbit IgG (H+L, 1:200), Texas Red conjugated goat anti-rabbit IgG (1:100) or Cy5 conjugated anti-rabbit secondary antibodies (1:200) (Jackson ImmunoResearch Laboratories, Inc.). SH-SY5Y cells were not stained, only studied with the confocal microscope for autofluorescence detection.

6 LC3-Adenovirus infections

CLN3 RNAi treated HUH7 cells were also used to study autophagy, which has been reported to be affected in Cln3 deficient cells (Cao et al., 2006). The autophagic marker was introduced by green fluorescent protein-conjugated LC3-Adenovirus (GFP-LC3-Ad) (Kochl et al., 2006) infection of cells, kindly provided by Sharon Tooze (Cancer Research UK, London Research Institute, Secretory Pathways Laboratory, London, UK) and amplified by myself while carrying out practical training. Infections were done with 100 virus particles per cell, on 5×10^5 cells that were transfected with siRNA twice before infection (trasfections as described before, infection one day after the last transfection). 24 hours later, the cells were starved in (induces autophagosome formation) Earle's Balanced Salt Solution (EBSS) + 10mM HEPES pH 7.4 for 30, 60 and 120 minutes. The starved cells were fixed for 20 minutes with 4% paraformaldehyde (PFA) in phosphate buffered saline (PBS) and permeabilized with 0.2% saponin. In order to distinguish autofluorescence from GFP-conjugated LC3, GFP was stained with 1:500 polyclonal rabbit GFP primary antibody (Santa Cruz Biotechnology) and 1:200 goat anti-rabbit secondary antibody (IgG) conjugated with Texas Red (Jackson ImmunoResearch Laboratories, Inc.). Lysosomes were stained with 1:100 diluted mouse monoclonal anti-human lysosomal membrane glycoprotein (LAMP1) primary antibody (H4A3, Developmental Studies Hybridoma Bank) and 1:200 goat anti-mouse secondary antibody (IgG) conjugated with Cy5 (Jackson ImmunoResearch Laboratories, Inc.).

7 Western Blot

After GFP-LC3-Ad infection and starvation, the cells were collected for Western blotting with 2×Laemmli sample buffer containing 2.5% β-mercaptoethanol. The sample proteins were separated in 11% SDS-polyacrylamide gel and blotted on Hybond-C nitrocellulose membrane (Amersham Biosciences/GE Healthcare). Non-specific binding of antibodies was suppressed by incubating the membrane for 60 min at room temperature (RT) in blocking buffer (5% milk in 1×Tris-Buffered Saline Tween-20 [TBST: 50mM Tris-HCl pH 7.4, 150mM NaCl, 0.05% Tween-20]). The primary antibody (mouse monoclonal GFP antibody, Santa Cruz Biotechnologies) diluted 1:1000 in the blocking buffer was bound by incubating again for 60 min at RT. Unbound antibodies were washed away by incubating once for 15 min and twice for 5 min RT in washing buffer (1×TBST). Primary antibodies were further labeled with a secondary antibody (horseradish peroxidase-conjugated polyclonal goat anti-mouse immunoglobulin, Daco Cytomation) diluted 1:5000 in 1×TBST, by incubating 30 min RT. Unbound antibodies were washed away by incubating three times for 5 min at RT in washing buffer. Proteins were detected with enhanced chemiluminescence system (ECL™, GE Healthcare) and visualized on X-ray films (Fuji Super RX medical, Fujifilm).

8 Microscopy

Phase contrast images showing the cell morphology of the previously mentioned three main cell lines were taken with an Axioplan 2 microscope. All the confocal images were taken with a Leica TCS SP1 confocal microscope. Adobe Photoshop and Adobe Illustrator CS softwares were used for image processing and figure assembly.

RESULTS

1 Silencing of *CLN3* in HEK293, HUH7 and SH-SY5Y cells

RNAi has previously been successfully used to inhibit *CLN3* expression in HeLa (human cervical cancer) cells, resulting in 91-96% down-regulation of the *CLN3* mRNA levels compared to scrambled control-siRNA (Pohl et al., 2007). In this study we used RNAi for the inhibition of *CLN3* expression in three other cell lines: HEK293, HUH7 and SH-SY5Y. The human embryonic cell line (HEK293) was chosen because this cell type is well characterized and easy to transfect. For this cell line, there were also previously optimized RNAi instructions available via Applied Biosystems. The human hepatoma cell line (HUH7) was chosen according to our interest in studying functional consequences of *CLN3* down-regulation, including abnormalities in autophagocytosis connected to JNCL. Autophagocytosis is a cellular function that can be easily induced experimentally, especially in the liver cells such as hepatoma cells. Autophagocytosis can thus be induced by starvation with amino acid or serum depletion. The human neuroblastoma cell line (SH-SY5Y) was chosen to represent neuronal cells since NCL disorders show most dramatic phenotype in neurons. The morphology of the selected cell types is shown in phase contrast pictures (see Figure 4A-C).

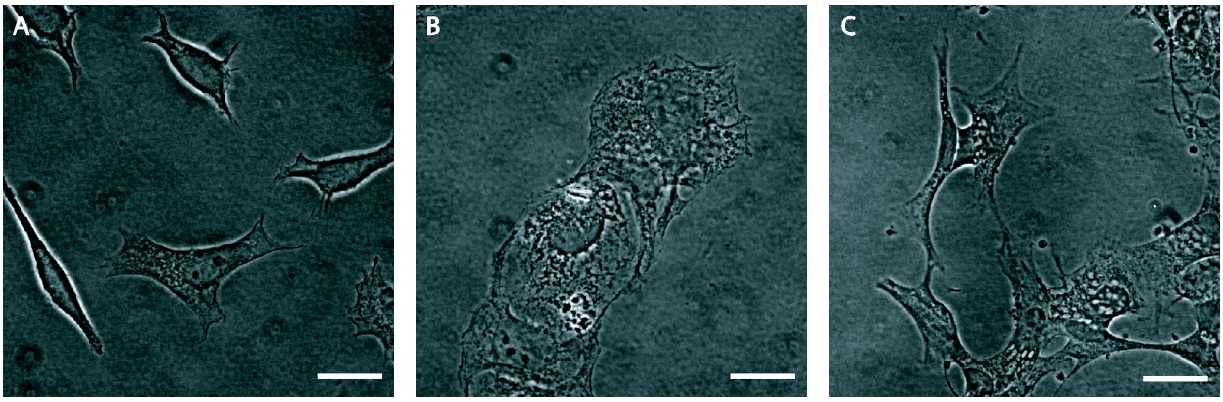

Figure 4 Phase contrast pictures of the cell lines used in the RNAi experiments. **A**: HEK293 cells, **B**: HUH7 cells and **C**: SH-SY5Y cells. Scale bar: 20µm.

1.1 Transfection of the RNAi oligos

Liposome-mediated siRNA transfections were optimized for the three distinct cell lines. This was accomplished with fluorescein-labeled dsRNA oligomers that emit light on wavelengths that can be detected as green colour with fluorescence microscopy. The transfection efficiency of these fluorescent siRNAs with the transfection reagent, could be optimized to about 90% (data not shown), along with the lowest possible dislocation rate of cells from the surface of the culture wells. This dislocation could possibly be caused by toxic effects resulting from excess amounts of the transfection reagent. The toxic effects could be detected as large vacuoles inside the cells, and avoided by optimizing the transfections. After optimization experiments, siRNA transfections were performed with the optimized amounts of transfection reagent and siRNA molecules. For the *CLN3* down-regulation experiments, the two siRNAs (siRNA-Ex6 and -Ex10) were transfected together in the same transfection media, either once or twice, depending on the experiment. The aim of simultaneous introduction of the two siRNA oligos targeted on two different exons was to inhibit *CLN3* expression more efficiently, since the *CLN3* gene codes for many different splice variant mRNAs. Therefore, the utilization of two siRNAs targeted to different exons was considered to interfere with a more extensive number of these variants. As a control for the effects caused by the transfections, a non-specific control-siRNA was transfected to cells in separate wells.

1.2 Standard curves

RNAs were extracted two days (Day 2), four days (Day 4) and six days (Day 6) after the first transfection (see Figure 5). If a second transfection was made, it was performed two days after the first transfection (on Day 2) and the RNAs extracted two and four days after the second transfection (on Day 4 and 6, see Figure 5). RNA extractions resulted in adequate concentrations and good quality ($A_{260/280}$ between 2.0-2.1, data not shown). To test the possible fragmentation of the RNA, a couple of the samples (HUH7 CLN3-siRNA Day 2, Day

4 and Day 6) were analyzed with Bioanalyzer. The data showed RNA Integrity Number (RIN) of 10.0 for all of the three samples, the highest value for integrity (see Figure 6). cDNAs from total mRNAs were produced with reverse transcription PCR. This first step of the two-stepped PCR produced only one strand of the cDNA, which was then used as a template for TaqMan real-time PCR.

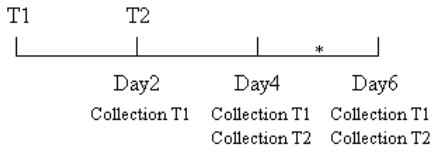

Figure 5 The time-points of the experiments. T1: first transfection (Day 0). T2: second transfection (Day 2). *: the time-point of GFP-LC3-Ad infection.

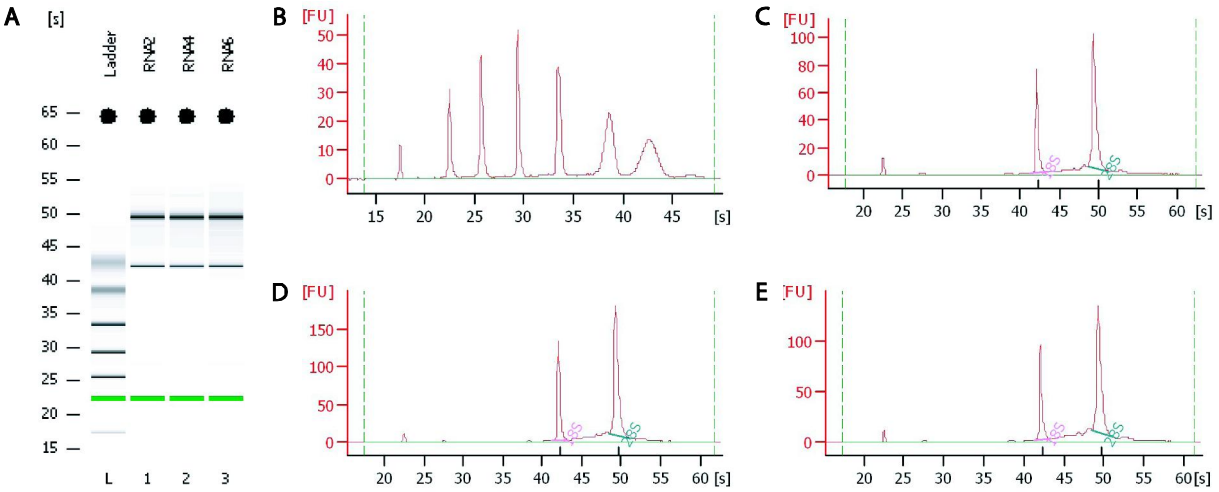

Figure 6: RNA integrity measured by Bioanalyzer. HUH7 samples from Day 2, Day 4 and Day 6 were used. **A:** Molecular size analysis of all the samples. **B:** Molecular weight marker, **C:** Day 2, **D:** Day 4 and **E:** Day 6. All the samples show the expected sharp 18S and 28S ribosomal RNA peaks and no fragmentation.

One of the cDNA samples from each cell type was chosen to perform TaqMan real-time PCR with dilution series for standard curve experiment preparation. Standard curve experiments were performed for each cell type and for some of them it had to be repeated for several times to obtain the correct concentrations (as an example, see Figure 7 for correct amplification of triplicates analyzed by 7000 System Software). Preparing standard curves for the experiments

enabled validation of PCR efficiency by comparison between the *CLN3* gene (this is the "target" gene) and endogenous control gene, *TBP*, expression (this is the "reference" gene used for normalization) and measuring the Pearson correlation co-efficient (r), which is the measure of the strength and direction of a linear relationship between the two variables (see results in Table 2 and Figure 8). The measures were determined according to Applied Biosystems instructions (see Table 2, Equation 4 and Equation 5). In order to get reliable results, the Pearson correlation coefficient (r) was required to reside between the values 1 and 0.95 (see Figure 8) and the slope difference between target (*CLN3*) and endogenous control (*TBP*) was optimized to reside below value 0.1, which was acquired for all the three different cell types (see Figure 9A-C).

$$\Delta Ct = Ct_{target} - Ct_{reference} \quad \textbf{4}$$

$$s = (s_1^{\,2} + s_2^{\,2})^{1/2} \quad \textbf{5}$$

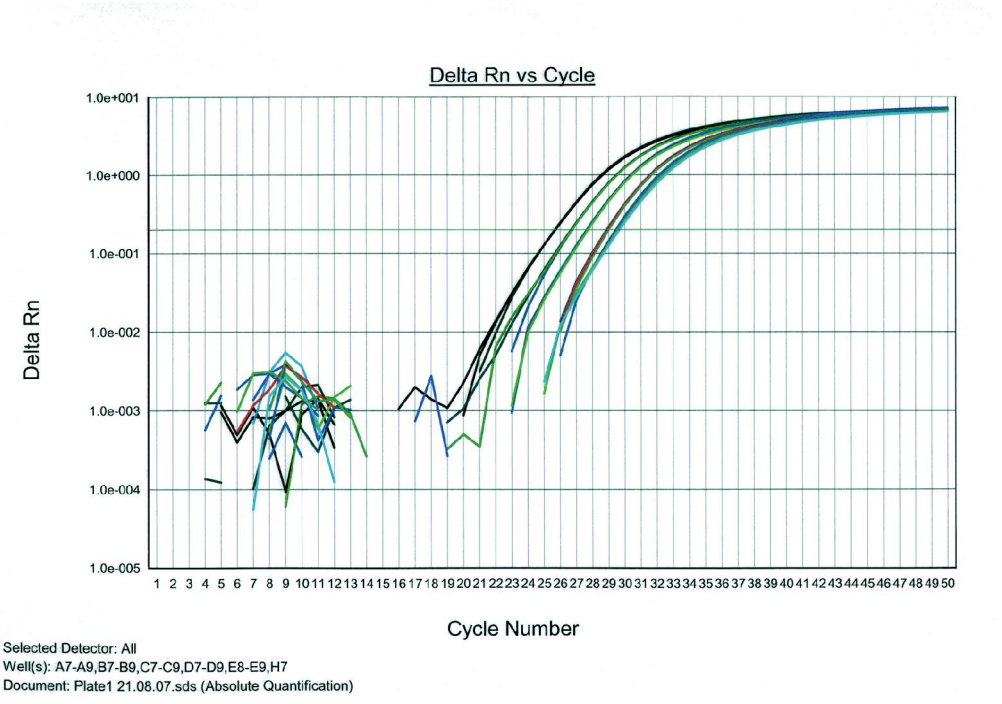

Figure 7: Amplification plots of five dilutions with triplicates showing optimal conditions. This figure is acquired from 7000 System software data of a standard curve experiment with HEK293 cells.

Table 2 Ct, ΔCt and standard deviation values for standard curve experiments.

		CLN3		*TBP*		*CLN3-TBP*	
	Qty (ng)	Average Ct	StdDev Ct	Average Ct	StdDev Ct	ΔCt	StdDev ΔCt
HEK293	33.00	25.63	±0.02	27.21	±0.25	-1.58	±0.25
	16.50	26.66	±0.03	28.06	±0.04	-1.40	±0.05
	8.25	27.61	±0.05	29.26	±0.14	-1.65	±0.15
	4.13	28.90	±0.08	30.60	±0.11	-1.70	±0.14
	2.06	29.50	±0.12	31.05	±0.05	-1.55	±0.13
HUH	50.00	22.52	±0.12	24.41	±0.27	-1.89	±0.29
	25.00	23.79	±0.22	25.38	±0.21	-1.59	±0.30
	12.50	24.49	±0.23	26.26	±0.15	-1.77	±0.27
	6.25	25.45	±0.33	27.24	±0.14	-1.79	±0.36
	3.13	26.33	±0.05	28.13	±0.05	-1.80	±0.07
SH-SY5Y	50.00	23.75	±0.60	25.07	±0.51	-1.32	±0.78
	25.00	25.20	±0.20	25.67	±0.14	-0.47	±0.25
	12.50	26.20	±0.06	26.57	±0.11	-0.37	±0.12
	6.25	26.65	±0.43	27.48	±0.05	-0.83	±0.43
	3.13	27.05	±0.29	28.25	±0.11	-1.20	±0.31

Quantities (Qty) are given as the amount of RNA and the average Ct-values (the cycle number acquired at the threshold level) calculated from triplicates of a single sample. ΔCt and ΔCt Standard Deviation (StdDev) values have been calculated according to Equation 4 and Equation 5. Two values coloured with pink contain an average of only two values. The third ones from these samples were left out due to their divergence from the average values.

Real-time PCR efficiencies were calculated according to Equation 1 (see page 24). Optimal percentage values should be close to 100% but as can be seen from the results (Figure 9D), the efficiency for HEK293 cells was lower. The results for HUH7 and SH-SY5Y cells reach levels over 100%, which might indicate problems in sample quality or errors in pipetting.

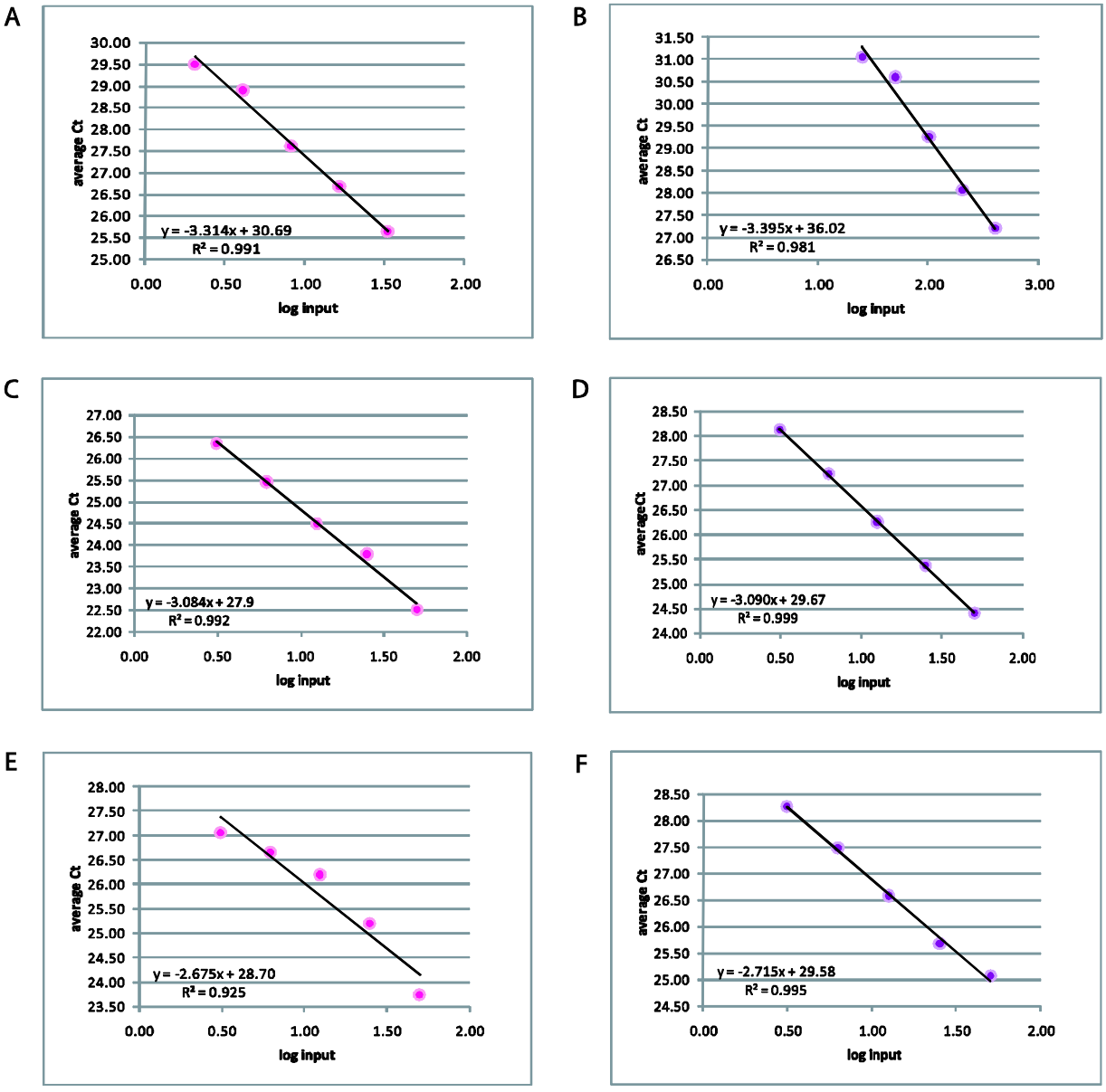

Figure 8 Standard curves acquired from real-time PCR. A: HEK293 CLN3, **B:** HEK293 TBP, **C:** HUH7 CLN3, **D:** HUH7 TBP, **E:** SH-SY5Y CLN3 and **F:** SH-SY5Y TBP. Values are a result of 2-fold dilution series with five different dilutions. Optimization for these standard curves was repeated until the slope difference (also represented in Figure 9) between *CLN3* and *TBP* in the same sample was below 1 and the Pearson correlation coefficient was between 0.95 and 1.

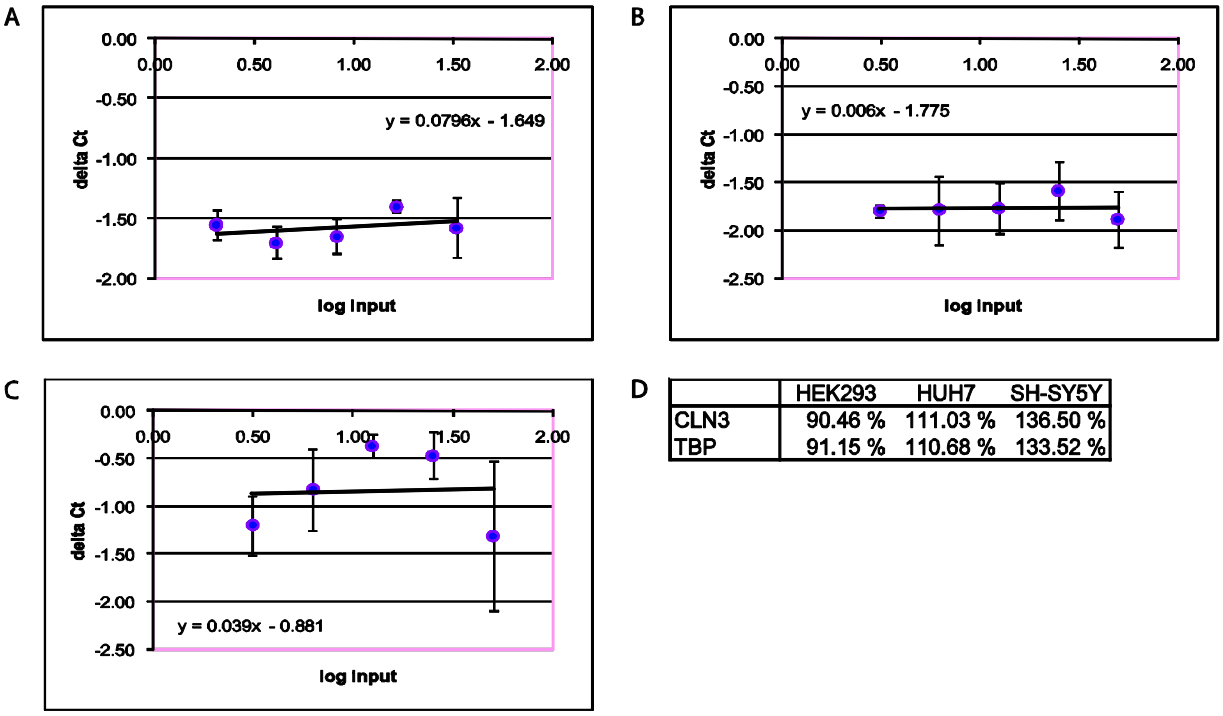

	HEK293	HUH7	SH-SY5Y
CLN3	90.46 %	111.03 %	136.50 %
TBP	91.15 %	110.68 %	133.52 %

Figure 9: Validation experiment and Real-time PCR efficiency. A: HEK293, **B:** HUH7 and **C:** SH-SY5Y. In this experiment 2-fold dilution series were produced from one of the cDNA samples, containing either TaqMan oligos for *CLN3* (target) or *TBP* (endogenous control). The values from dilution series amplifying *CLN3* have been subtracted with the reference values of amplified *TBP*. Target gene amplification values have thus been normalized for the values given by a non-targeted reference gene amplification. These ΔCt extracted values should be about the same and result in slope value under 0.1, as acquired for each cell line. **D**: These real-time PCR efficiency values/percentages have been calculated with Equation 1. The slope values have been acquired from the standard curve trendlines (see Figure 8). Applied Biosystems guarantees 100% efficiency for all of their TaqMan oligos used. According to the values in this figure, the expected efficiency is not truly reached or is exceeded in these experiments.

1.3 Quantitative real-time PCR analysis on HEK293 samples

The first RNAi experiments were carried out using HEK293 cells, with only one siRNA transfection including both of the two oligos that were targeted on exons 6 and 10 of *CLN3* encoded mRNAs. Total RNA for relative quantification of *CLN3* expression was extracted on days 2, 4 and 6 after the transfection (see Figure 5). All the calculations were performed according to the Applied Biosystems instructions by using the Equations 4-7; results from each calculation step are shown Tables 3 and 4. The qRT-PCR analysis revealed down-

regulation of *CLN3* in siRNA-transfected samples. The baseline for fold difference is 1, which was approximately the value observed for the reference samples that were not transfected with siRNAs ("control", see Table 4). Thus, all values above 1 indicate up-regulation of the analyzed gene expression. All the values between 0 (no expression) and 1 (normal expression) indicate down-regulation that can be converted to percentage values relative to the normal level. All the values observed from siRNA-transfected samples were below 1, indicating down-regulation of *CLN3*. When the standard deviation was taken into account, the control values were situated between the values 0.75 and 1.33. Therefore, the significant values for down-regulation or up-regulation were set to reside below 0.75 or above 1.33.

The results from calibrator samples that were transfected with non-specific siRNAs ("control-siRNA") should not show any significant fold changes on CLN3 mRNA levels measured by qRT-PCR. Regardless of their feature as non-acting siRNAs, the results did show some significant negative fold changes; 0.66 on each of the three days (see Table 4). This value can be converted to 34% reduction of *CLN3* expression compared to the control samples without any transfection (reference samples). Target samples, representing the actual *CLN3*-targeted siRNA transfections ("CLN3-siRNA"), show even larger changes in expression; 0.25, 0.27 and 0.30 (Table 4). These results can be converted to 70%, 73% and 75% reduction compared to the reference samples. From the expression ratios shown by these results, we could see that the mRNA levels resulting from *CLN3* expression had been down-regulated by the RNAi but not as much as expected. CLN3 mRNA-levels were detected to be lowest on the second day after transfection, but because the transfection was transient, the mRNA levels started slowly to rise after the second day (see Table 4 for average values). Because of the lack of an antibody that would be used for staining the endogenous CLN3 protein, we could not measure the protein levels by Western blotting and could only predict the time needed for protein turnover. The half life of CLN3 protein was also not known and the effect of siRNA mediated down-regulation of the protein could not be detected. Due to the slight rise of CLN3 mRNA levels after the transfection, a second transfection was planned for the following studies with HUH7 and SH-SY5Y cells, to keep the mRNA-levels down until the protein level decreases.

$$\Delta\Delta Ct = \Delta Ct_{testsample} - \Delta Ct_{calibratorsample} \quad \textbf{6}$$

$$2^{-(\Delta\Delta Ct \pm s} \quad \textbf{7}$$

Table 3 Ct, ΔCt and standard deviation values from HEK293 samples.

		CLN3		*TBP*		*CLN3-TBP*	
		Average Ct	StDev Ct	Average Ct	StDev Ct	ΔCt	StDev ΔCt
Day 2	Control	24.62	±0.20	26.61	±0.32	-1.99	±0.37
	Control-siRNA	24.87	±0.03	26.26	±0.10	-1.39	±0.10
	CLN3-siRNA	26.64	±0.01	26.65	±0.05	-0.01	±0.05
Day 4	Control	25.50	±0.12	26.99	±0.22	-1.49	±0.25
	Control-siRNA	25.36	±0.02	26.26	±0.06	-0.90	±0.06
	CLN3-siRNA	27.04	±0.03	26.65	±0.07	0.39	±0.08
Day 6	Control	26.46	±0.04	28.01	±0.19	-1.55	±0.20
	Control-siRNA	27.18	±0.04	28.14	±0.02	-0.96	±0.04
	CLN3-siRNA	27.49	±0.03	27.31	±0.09	0.18	±0.09

Quantities (Qty) are given as the amount of RNA and the average Ct-values (the cycle number acquired at the threshold level) calculated from triplicates of a single sample. ΔCt and ΔCt Standard Deviation (StdDev) values have been calculated according to Equation 4 and Equation 5.

Table 4 ΔΔCt, standard deviation and fold change values from HEK293 samples.

		ΔΔCt	StDev	Fold change	Average Fc
Day 2	Control	0.00	±0.37	0.77 - 1.30	1.03
	Control-siRNA	0.60	±0.10	0.62 - 0.71	0.66
	CLN3-siRNA	1.98	±0.05	0.25 - 0.26	0.25
Day 4	Control	0.00	±0.25	0.84 - 1.19	1.02
	Control-siRNA	0.59	±0.06	0.64 - 0.69	0.66
	CLN3-siRNA	1.88	±0.08	0.26 - 0.29	0.27
Day 6	Control	0.00	±0.20	0.87 - 1.15	1.01
	Control-siRNA	0.59	±0.04	0.65 - 0.68	0.66
	CLN3-siRNA	1.73	±0.09	0.28 - 0.32	0.30

ΔΔCt, standard deviation (StDev) and fold change values are calculated according to the Equation 6 and Equation 7. Average fold change (Fc) values show the final estimated change in target samples compared to the control. Normal level of expression show approximately the value of 1 and the changes outside the range 0.75-1.30 are considered as significant.

1.4 Quantitative real-time PCR analysis of HUH7 samples

In the RNAi experiments that were performed for HUH7 cells, second transfections (T2) were made two days after the first transfections (T1, see Figure 5). HUH7 cells were seeded between the transfections (on Day 1), due to the fast division and growth rate. RNAs were extracted on Days 2, 4 and 6 (see Figure 5). Unlike in the results from HEK293 cells, the qRT-PCR analysis showed variable results in repeated experiments (see Table 6). The results from the reference samples showed the expected value that resides within the range mentioned earlier (0.75<1.33) and is close to value 1. The fold changes detected from the calibrator samples (control-siRNA) showed controversial results. On Day 2, the calibrator sample showed down-regulation with value 0.46 (54%). This is not the value expected according to the rule that no significant changes should be detected for calibrator samples. On Day 4 this value was 0.67 (33%) which also represents significant down-regulation. On Day 6, on the other hand the control-siRNA value was detected as 1.72, which is fairly over the standard deviation limit acquired from the reference samples (1.33), thus indicating up-regulation of *CLN3*. These results indicate problems with the transfections, involving cellular changes resulting from too high concentrations of either transfection reagent or siRNAs. Non-specific induction of the innate immune system by the control-siRNA molecules might also be involved.

Results from the actual *CLN3*-targeted siRNA transfections showed quite high down-regulation of *CLN3* especially on Day 2, with only one transfection; 0.28 (72% see Table 6). This result might be false positive due to the unexpected results obtained for the calibrator samples. Values on Day 4 did not show high down-regulation (26% and 47%). These results do not significantly differ from the values on control-siRNA samples, indicating no specific *CLN3* knock-down on Day 4. Results on Day 6 show up-regulation by the factors of 1.59 and 2.25. From these results we could conclude that the RNAi experiment had not been completely successful for HUH7 cells and probably induced other effects in the cells that resulted in alteration of the *CLN3*-levels even in control-siRNA-treated samples.

Table 5 Ct, ΔCt and standard deviation values from HUH7 samples.

		CLN3		*TBP*		*CLN3-TBP*	
		Average Ct	StDev Ct	Average Ct	StDev Ct	ΔCt	StDev ΔCt
Day 2	Control	22.38	±0.14	24.80	±0.30	-2.42	±0.33
	Control-siRNA	23.33	±0.11	24.61	±0.20	-1.28	±0.23
	CLN3-siRNA T1	23.89	±0.27	24.45	±0.20	-0.56	±0.34
Day 4	Control	23.52	±0.24	25.66	±0.16	-2.14	±0.28
	Control-siRNA	23.21	±0.19	24.73	±0.26	-1.52	±0.32
	CLN3-siRNA T1	22.73	±0.10	24.43	±0.12	-1.70	±0.16
	CLN3-siRNA T2	23.42	±0.21	24.60	±0.29	-1.18	±0.36
Day 6	Control	23.25	±0.23	24.41	±0.08	-1.16	±0.24
	Control-siRNA	22.51	±0.32	24.37	±0.37	-1.86	±0.49
	CLN3-siRNA T1	22.32	±0.23	24.11	±0.27	-1.79	±0.35
	CLN3-siRNA T2	22.57	±0.07	24.89	±0.14	-2.32	±0.15

Quantities (Qty) are given as the amount of RNA and the average Ct-values (the cycle number acquired at the threshold level) calculated from triplicates of a single sample. ΔCt and ΔCt Standard Deviation (StdDev) values have been calculated according to Equation 4 and Equation 5.

Table 6 ΔΔCt, standard deviation and fold change values from HUH7 samples.

		ΔΔCt	StDev	Fold change	Average Fc
Day 2	Control	0.00	±0.33	0.79 - 1.26	1.03
	Control-siRNA	1.14	±0.23	0.39 - 0.53	0.46
	CLN3-siRNA T1	1.86	±0.34	0.22 - 0.35	0.28
Day 4	Control	0.00	±0.28	0.82 - 1.22	1.02
	Control-siRNA	0.62	±0.32	0.52 - 0.81	0.67
	CLN3-siRNA T1	0.44	±0.16	0.66 - 0.82	0.74
	CLN3-siRNA T2	0.96	±0.36	0.40 - 0.66	0.53
Day 6	Control	0.00	±0.24	0.84 - 1.18	1.01
	Control-siRNA	-0.70	±0.49	1.15 - 2.29	1.72
	CLN3-siRNA T1	-0.63	±0.35	1.21 - 1.97	1.59
	CLN3-siRNA T2	-1.16	±0.15	2.01 - 2.48	2.25

ΔΔCt, standard deviation (StDev) and fold change values are calculated according to the Equation 6 and Equation 7. Average fold change (Fc) values show the final estimated change in target samples compared to the control. Normal level of expression show approximately the value of 1 and the changes outside the range 0.75-1.30 are considered as significant.

1.5 Quantitative real-time PCR analysis of SH-SY5Y samples

SH-SY5Y cells were also transfected twice, in the same manner as HUH7 cells. The SH-SY5Y cells were not seeded between the transfections, according to the slower division time and poor adhesion rate to the well surface by the cells that had been transfected once. SH-SY5Y cells can grow both as adherent cells but also in solution, making the rate of adhesion even slower. Fold changes measured by qRT-PRC showed controversial results. The values for non-transfected control samples showed the expected results (relative CLN3 mRNA levels were between 0.75 and 1.33) but the values for the siRNA-transfected samples were to some extent inconsistent. The results for calibrator samples showed down-regulation on Day 2 (0.81; 19%), significant down-regulation on Day 4 (0.29; 71%) and up-regulation on Day 6 (1.95-fold). Only the result on Day 2 could be considered as relevant.

The *CLN3*-targeted siRNA transfections also yielded non-expected results. On Day 2 the down-regulation was only 30% (0.70), on Day 4 there was less down-regulation than on the calibrator sample: 38% (0.62) with one transfection and 58% (0.42) with two transfections. On Day 6 the results were: 30% (0.70) down-regulation after one transfection and 43% (0.57) after two transfections. The results especially on Day 4 and 6 were considered to be unreliable, due to the peculiar results of the calibrator samples. All the results from HEK293, HUH7 and SH-SY5Y samples are summarized in Figure 10.

Table 7 Ct, ΔCt and standard deviation values from SH-SY5Y samples.

		CLN3		*TBP*		*CLN3-TBP*	
		Average Ct	StDev Ct	Average Ct	StDev Ct	ΔCt	StDev ΔCt
Day 2	Control	23.10	±0.10	24.61	±0.38	-1.51	±0.39
	Control-siRNA	23.11	±0.08	24.31	±0.19	-1.20	±0.20
	CLN3-siRNA T1	23.06	±0.06	24.04	±0.15	-0.98	±0.16
Day 4	Control	23.18	±0.06	24.16	±0.29	-0.98	±0.29
	Control-siRNA	25.88	±1.34	24.52	±0.27	1.36	±1.36
	CLN3-siRNA T1	24.60	±0.11	24.83	±0.37	-0.23	±0.39
	CLN3-siRNA T2	25.13	±0.20	24.81	±0.37	0.32	±0.42
Day 6	Control	25.17	±0.27	25.94	±0.31	-0.77	±0.41
	Control-siRNA	24.32	±0.20	25.90	±0.65	-1.58	±0.68
	CLN3-siRNA T1	25.65	±0.23	25.83	±0.42	-0.18	±0.48
	CLN3-siRNA T2	25.82	±0.23	25.73	±0.33	0.09	±0.40

Quantities (Qty) are given as the amount of RNA and the average Ct-values (the cycle number acquired at the threshold level) calculated from triplicates of a single sample. ΔCt and ΔCt Standard Deviation (StdDev) values have been calculated according to Equation 4 and Equation 5.

Table 8 ΔΔCt, standard deviation and fold change values from SH-SY5Y samples.

		ΔΔCt	StDev	SH-SY5Y	Average
Day 2	Control	0.00	±0.39	0.76 - 1.31	1.04
	Control-siRNA	0.31	±0.20	0.70 - 0.93	0.81
	CLN3-siRNA T1	0.53	±0.16	0.62 - 0.77	0.70
Day 4	Control	0.00	±0.29	0.82 - 1.22	1.02
	Control-siRNA	2.34	±1.36	0.08 - 0.51	0.29
	CLN3-siRNA T1	0.75	±0.39	0.45 - 0.78	0.62
	CLN3-siRNA T2	1.30	±0.42	0.30 - 0.54	0.42
Day 6	Control	0.00	±0.41	0.75 - 1.33	1.04
	Control-siRNA	-0.81	±0.68	1.10 - 2.81	1.95
	CLN3-siRNA T1	0.59	±0.48	0.48 - 0.92	0.70
	CLN3-siRNA T2	0.86	±0.40	0.42 - 0.73	0.57

ΔΔCt, standard deviation (StDev) and fold change values are calculated according to the Equation 6 and Equation 7. Average fold change (Fc) values show the final estimated change in target samples compared to the control. Normal level of expression show approximately the value of 1 and the changes outside the range 0.75-1.30 are considered as significant.

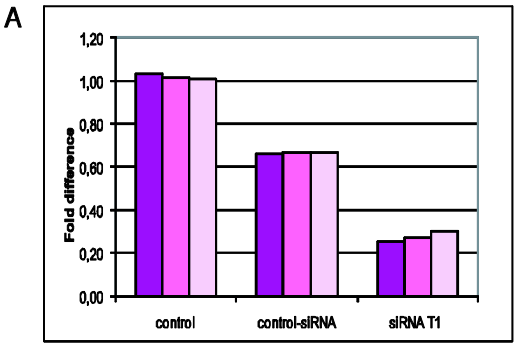

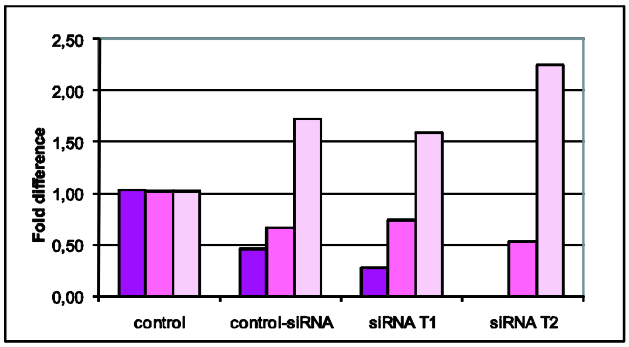

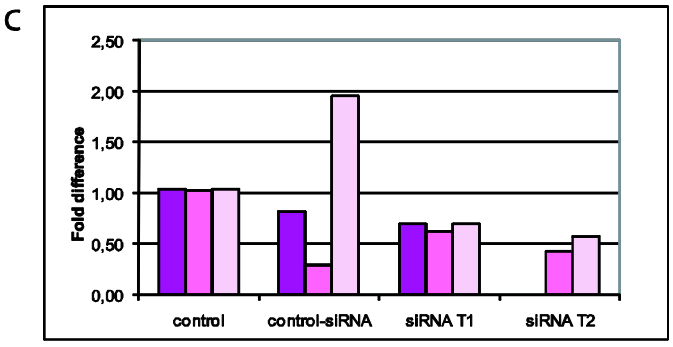

D

		HEK293	HUH7	SH-SY5Y
Day 2	control	1.03	1.03	1.04
Day 4		1.02	1.02	1.02
Day 6		1.01	1.01	1.04
Day 2	control-siRNA	0.66	0.46	0.81
Day 4		0.66	0.67	0.29
Day 6		0.66	1.72	1.95
Day 2	siRNA T1	0.25	0.28	0,70
Day 4		0.27	0.74	0.62
Day 6		0,30	1.59	0,70
Day 4	siRNA T2		0.53	0.42
Day 6			2.25	0.57

Figure 10: Summary of the qRT-PCR results. A: HEK293, **B**: HUH7, **C**: SH-SY5Y and **D**: average fold differences represented as numbers, summarized from Table 4**,** Table 6 and Table 8. Different colors of the columns represent the different days on which the cells were collected for RNA extraction. **Purple**: two days after the first transfection (Day 2). **Pink**: four days after the first transfection and in the siRNA T2 columns, two days after the second transfection (Day 4). **Light pink**: six days after the first transfection and in the siRNA T2 columns, four days after the second transfection (Day 6). T1 means one transfection (on Day 0) and T2 two transfections (on Day 0 and Day 2).

2 Detection of the NCL markers in RNAi treated cells

The RNAi experiments in different cell lines were performed also for fluorescence microscopy studies. The main aim of the *CLN3*-targeted RNAi was to monitor whether the typical markers for NCLs: the accumulation of autofluorescent lipopigment and the subunit c of mitochondrial ATP synthase (SCMAS), could be detected in RNAi-treated cells versus the control cells. The currently available antibodies against the hydrophobic SCMAS are poor, and during the immunofluorescent labelling experiments it became clear that the SCMAS antibody was not

able to detect possible accumulation in RNAi-treated cells. SCMAS was thus left out from the characterization.

Accumulation of autofluorescent lipopigments can be detected on the FITC-channel with the confocal microscope. The autofluorescence might be difficult to interpret in cells with a high division rate, due to the possible longer time scale required for the accumulation to form. The immunofluorescence studies showed no accumulation of autofluorescent lipopigments in HEK293 or SH-SY5Y cells (data not shown). To confirm the detection method for the autofluorescent NCL marker, we also used fibroblasts from *Cln3* knockout mice that have been reported to show accumulation of autofluorescent lipopigment. These cells and control fibroblasts were treated with leupeptin (a protease inhibitor) and hypertonic media (fluid removal) to improve detection of the autofluorescent lipopigment accumulation but no accumulation was observed in these cell either. Instead, major accumulation of autofluorescence was detected in the RNAi-treated HUH7 cells; two days after the second transfection (Day 6, see Figure 11). These results were somewhat contradictory, since according to the qRT-PCR results the down-regulation of *CLN3* was not successful on Day 6. Instead, the results showed up-regulation of *CLN3* (see Figure 10 for a review). The lipofectamine transfection reagent can also give autofluorescence, which might also give the same result as in Figure 12 B. For this reason, the control cells should have also been treated with the transfection reagent. Although the results from qRT-PCR did not show down-regulation of *CLN3* on Day 6, it might be possible that the down-regulation detected from the Day 2 samples caused effects on the cells (such as the autofluorescence accumulation), that were not restored as quickly as the *CLN3* mRNA-levels.

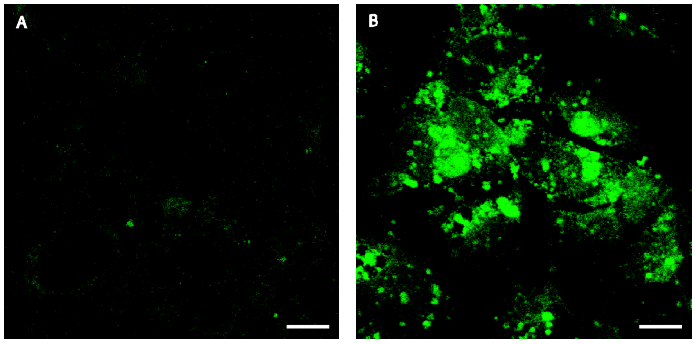

Figure 11: Confocal microscope visualization of autofluorescence in HUH7 cells. **A**: Control cells without siRNA transfection. **B**: Cells with *CLN3*-targeted siRNA transfection showing massive autofluorescence accumulation on day 6. Scale bar: 10µm.

3 Detection of autophagy in RNAi-treated cells

The utilization of siRNA-treated cells for functional studies was tested with the detection of autophagy in HUH7 cells. The aim was to detect possible disturbance at the fusion of lysosomes and autophagosomes of *CLN3*-knock down cells. HUH7 cell line was chosen instead of HEK293 or SH-SY5Y because autophagy is easily induced in the cell line. The cells were transfected with *CLN3*-siRNA or control-siRNA and infected with GFP-LC3-Adenovirus one day after the second siRNA transfection (Day 5, see * in Figure 5). LC3 is a microtubule-associated protein, which was introduced into the cells by adenoviral transduction. It is a commonly used marker for autophagosomes and can be easily detected when fused with green fluorescent protein (GFP). One day after the infection (Day 6), autophagy was induced by 30, 60 or 120min starvation with amino-acid and serum free medium. The cells were fixed and stained for the confocal microscopy. Lysosomes were stained to detect their colocalization with the formed autophagosomes. However, analysis with the confocal microscopy showed similar phenotype for the control-siRNA and *CLN3*-siRNA transfected cells with pathological effects. The morphology of the both RNAi-treated cells (control-siRNA and CLN3-siRNA) was clearly changed compared to the morphology of non-treated control cells (data not shown). All the cells subjected to siRNA transfection and GFP-

LC3-Ad infections showed large vacuoles in the cytoplasm even before starvation to induce autophagy (Figure 12). Therefore, the siRNA transfections followed by LC3-GFP-adeno infections seemed to cause too much stress for the cells and therefore were not useful for these functional studies. We could not detect clear green autophagosomal vacuoles either (as seen in Figure 13, ctrl starv), even though the cytoplasm of the starved control cells, showed some dark vacuoles. These studies were repeated, giving comparable results.

Previous studies have shown that, during starvation soluble LC3-I is cleaved and modified by addition of a lipid group, forming LC3-II (Kochl et al., 2006), which is considered as a marker of pre-autophagosomes. This lipidation of LC3 can be detected by Western blotting, due to the altered size of the modified protein. Accordingly, the amount of LC3-II should be increased in the siRNA-treated cells because the formation of autophagosomes has been reported to be enhanced in the previously studied *Cln3* deficient cells (Cao et al., 2006). Lysates from the LC3-GFP-infected and siRNA-transfected cells described above were Western blotted but did not show any significant size changes in the LC3 bands compared to the control samples (data not shown).

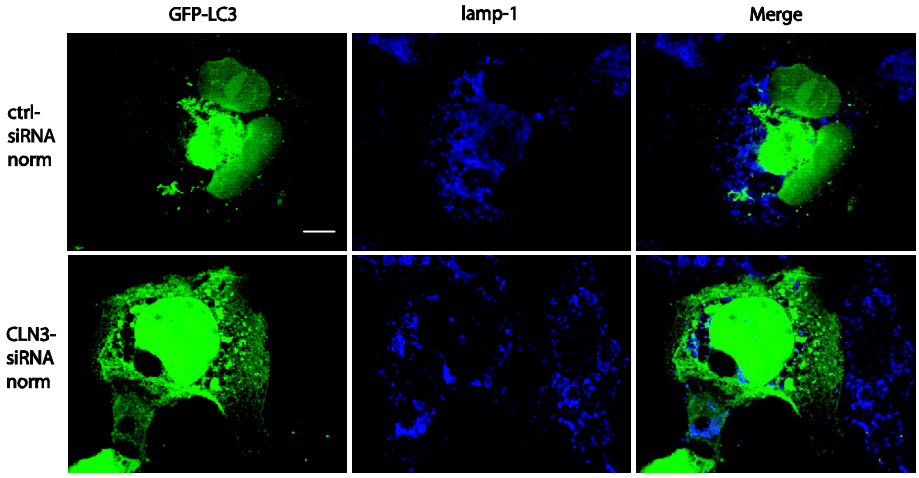

Figure 12: Induced autophagocytosis in HUH7 cells with CLN3-siRNA transfections and GFP-LC3-Adenovirus infections. The first column shows expression of GFP-LC3, which is a marker for autophagosomes. The possible autofluorescent lipopigment accumulation overlaps the GFP emission and is also detected with the same channel (immunostaining of GFP in order to extract it from autofluorescence did not succeed). The second column shows staining of lamp-1, which is a lysosomal marker. In the last column, these two channels are merged. Abbreviations; norm: normal media (control). Scale bar: 10µm.

DISCUSSION

RNAi is a complex cellular process and not easily achieved in all cell types or cell lines. This is noteworthy especially in mammalian species where long dsRNAs induce interferon effects and therefore only short dsRNAs, such as siRNAs, can be used to induce RNAi responses. All of the three cell lines used in this study are well characterized and widely used in cell biological studies and RNAi experiments with siRNA transfections have been performed for all of them (Ahn et al., 2003; Chang and Taylor, 2003; Taira et al., 2004). The results obtained in these studies did not show as high down-regulation of *CLN3* as expected, in any of the three cell lines used. The qRT-PCR results from HEK293 cells showed the most even and reliable results but not sufficient down-regulation of *CLN3*. The qRT-PCR data obtained from HUH7 and SH-SY5Y cells showed conflicting results partly due to the unexpected values in control-siRNA samples. Even though the qRT-PCR did not confirm accurate down-regulation of *CLN3* in HUH7 cells, apparent accumulation of autofluorescent lipopigment was detected in the phenotypic studies. This phenotypic marker was not detected in HEK293 or SH-SY5Y cells. In functional studies, the siRNA transfections combined with GFP-LC3-Ad infections seemed to cause excess stress to the HUH7 cells. Therefore, cytopathic effects were detected in the cells which were both transfected and infected.

In the present studies, reasonably efficient down-regulation of *CLN3* with RNAi was achieved only in the HEK293 cells, with 70-75% knock-down compared to the untransfected control. Thus, the expression of *CLN3* was not completely inhibited and did not reach the levels reached in the HeLa studies, where the target down-regulation caused by specific siRNA transfections was compared to the data acquired from scrambled siRNA control samples and resulted in 96-99% down-regulation of *CLN3* (Pohl et al., 2007). The results obtained from the HEK293 cells were not completely reliable, since the control-siRNA transfections also resulted in significant down-regulation, although at much lower levels (34%). Compared to the control value, the actual down-regulation by the *CLN3*-specific siRNA transfections would be even less effifient. These values do not indicate sufficient down-regulation of *CLN3* in

HEK293 cells. In the future, the control cells giving gene expression values for calibrator samples should be incubated with the transfection reagent without any siRNA, to determine the effect specifically caused by the utilization of the transfection reagent. Thus, the vehicle should be included in the control. The results for the HUH7 and SH-SY5Y samples were controversial due to the inconsistent data acquired from the control-siRNA-treated reference samples. Because the values vary between the samples from different days, it might indicate non-specific modification of mRNAs via induction of the innate immune system, caused by the control-siRNA molecule or by the effects caused by the transfection reagent. In the future, it would be recommendable to use at least two different control-siRNAs to exclude the effect of possible immune responses. Other transfection reagents should also be tested.

When considering the problems encountered in qRT-PCR, one of the topics to be contemplated would be the validity of TaqMan experiments. The efficiency of these experiments was validated by the standard curve method; it was slightly less than 100% for HEK293 samples and fairly over 100% for HUH7 and SH-SY5Y samples. These standard curve experiments are not commonly performed when using the Comparative Ct Method with TaqMan primers, since the manufacturer quarantees 100% efficiency for all of their primers. We wanted to test the efficiencies and to define optimal concentrations of the samples used for the experiments. An attempt was made to eliminate all the error-causing factors during the experiments by accepting only high quality extracted RNAs and by using an automated pipet for the reaction plate preparations. The PCR efficiency on the HEK293 samples could have been increased by optimizing reaction temperatures or by trying different TaqMan probes and primers. The PCR efficiency problems with the HUH7 and SH-SY5Y samples might indicate errors in pipetting or in sample quality. However, pipetting errors were reduced to a minimum by using an automatic pipettor and the RNAs should have a high quality, as detected by the Bioanalyzer (see Figure 6). There might have been some DNA contaminations in the samples but they should not give any false results since the TaqMan primers were designed on exon-exon boundaries, thus amplifying only mRNAs and excluding amplification of genomic DNA. The TaqMan qRT-PCR accuracies were verified with the control samples without any

transfection, and gave the expected values that resided approximately at the baseline value 1. These results give a stable basis on which the results from samples with transfections can be compared. Thus, the problems must be caused by other factors than the TaqMan method. According to the results obtained from the enhanced end-point PCR test, we can also conclude that even though this method would be much cheaper, one can not achieve accurate quantitative results with it.

Considering the facts discussed above, the next question would be the accuracy of target gene down-regulation with the two siRNAs. The advantage of using simultaneously two siRNAs targeted on two different exons would be the RNAi-targeting of more splice variants. The disadvantage of this method is the possible saturation of the RNAi machinery with excess siRNAs or competitive inhibition between the two siRNAs. Off-target effects can also occur with related sequences. Since the obscure results were obtained also from the non-specific siRNA-transfected samples that basically set the basis for indentifying changes made by the transfections, the main problem might be solved by considering the transfection protocols.

All the transfections were performed with lipofectamine, which utilizes cationic liposomes for nucleic acid internalization. For HEK293 cells, qualified instructions could be found from the Invitrogen internet pages, making the optimization easier. For HUH7 and SH-SY5Y cells, the transfections had to be optimized more carefully and the excess use of lipofectamine resulted in formation of vacuoles in the cytoplasm. It is also known that the excessive use of siRNA can harm the cell viability. Therefore, the most probable reason for the inexact results obtained in q-PCR might have been the excess use of lipofectamine and/or siRNA. For future studies, a cell viability test before RNA extractions should be employed. In SH-SY5Y cells, one of the problems conserning cell attachment and viability could have been the wrong composition of media. After adding on the 0.1% non-essential amino acids, the cells seemed to grow and attach better to the surface of the growth flasks. The composition of the culture media was tested according to new information after the experiments performed for this master’s thesis.

Another method for quantifying accumulating phenotypes would be the use of stable RNAi, perhaps by the lentiviral system. This would allow the constant inhibition of the target gene, in which case multiple transfections would not be needed and incubation times to allow accumulation of NCL markers would be possible even in cell lines with fast division rates. These stable infections might also help when performing functional studies involving viral infections. Lack of the second transfection might better maintain the cell viability.

Phenotypic observation of autofluorescent lipopigment accumulation did not show positive results in HEK293 cells, questioning the down-regulation obtained from the qRT-PCR. As the accumulation of this NCL marker was tested also with *Cln3*-knockout fibroblasts without any positive results observed two days after the seeding, the incubation time required for this phenotype to appear was considered. The characteristic autofluorescence accumulation has been detected in knockout neuronal cells after four days of incubation (Hughes et al., 1999), which might indicate that two days is not enough for the accumulation to form in the fast-dividing HEK293 cells. The requirement for long growth periods might be problematic when considering a cell line optimal both for transient RNAi experiments and phenotypic studies. Although the values from qRT-PCR on HUH7 samples showed controversial results and even up-regulation of *CLN3* in siRNA-transfected cells, the phenotypic studies showed accumulation of autofluorescent lipopigments. Therefore, it is possible that the RNAi was succesful after all, at least for the cells used in immunofluorescence studies. The reason why efficient and lasting down-regulation was not detected in the samples for qRT-PCR is not known. HUH7 cells might be better for this sort of phenotypic studies, because they have a somewhat slower division rate than HEK293 cells or they might be sensitive for even mild down-regulation of *CLN3* levels. However, the difference is not large, making it unclear why such a strong phenotypic change can be observed especially in the HUH7 cells. The autofluorescence caused by the lipofectamine might also take part. The SH-SY5Y cells were expected to give optimal results at least in the phenotypic studies but according to the results from qRT-PCR, the siRNA transfection is not well functional in these cells. SH-SY5Y cells have even slower division-rate than HUH7 cells and would have been probably the most

appropriate model for NCL, also due to their neuronal origin. For phenotypic analysis of NCL, perhaps some other markers than autofluorescent accumulation should be considered that might allow analysis without long incubation periods after siRNA-treatments.

Due to the lack of clear GFP-LC3-positive vacuoles in the starved control cells, we can conclude that the induction of autophagy had not been effective. Compared to the control cells only infected with GFP-LC3-Ad, the cells treated with either non-specific siRNA or *CLN3*-targeted siRNA both showed clear effects on cell morphology. In a previous study, the GFP-LC3-Ad infections and siRNA transfections had been performed in the opposite order (Ding et al., 2007). In future studies, this order could be relevant when studying autophagy in siRNA-transfected cells, and the starvation conditions should be optimized further.

One advantage in this type of RNAi studies would be the ability for direct observation of disease phenotype in human cells, without requirement for patient cells or mouse models. As many of the cell biological studies have been performed in cells derived from knock-out mouse models, the results can fairly well represent the disease phenotype that would be expressed in human cells with NCL disorder. However, cellular processes can vary between mouse and human. It may therefore be hard to draw generalized conclusions from functional experiments in cells of one species. Other problems perhaps connected especially to NCL mouse models are the possible compensatory pathways circumventing the effects of the disease protein in these model organisms. Over the time of development or passing through generations of the knock-out mice, there might be some other proteins expressed that can compensate for the effects caused by the mutated NCL protein and thus alter the pathways. This could render the obtained phenotype milder than expected and disturb the experimental setup. Especially in transient siRNA transfection systems and also in stable siRNA expression systems, these effects can be bypassed. In an optimal RNAi the gene expression will be silenced, possibly creating a different situation than in a real NCL cell. In the case of *CLN3*, the mutated gene codes for a truncated protein that retains to the ER and is not targeted to the lysosomes. However, these truncated proteins seem to have a function related to the size of the

lysosomes (Kitzmuller et al., 2008). If this assumption is correct, then the research set-up in siRNA-treated cells would not give a truthful illustration of the diseased cell phenotype. Therefore, further studies using RNAi possibly in different cell types, with different transfection methods and alternative phenotype markers are needed for the preparation of large scale systems such as genome-wide RNAi technologies and phenotypic screenings for NCLs.

REFERENCES

http://www.ninds.nih.gov/disorders/encephalopathy/encephalopathy.htm, 11.01.2008

Ahn, S., C.D. Nelson, T.R. Garrison, W.E. Miller, and R.J. Lefkowitz. 2003. Desensitization, internalization, and signaling functions of beta-arrestins demonstrated by RNA interference. *Proc Natl Acad Sci U S A*. 100:1740-4.

Ahtiainen, L., O.P. Van Diggelen, A. Jalanko, and O. Kopra. 2003. Palmitoyl protein thioesterase 1 is targeted to the axons in neurons. *J Comp Neurol*. 455:368-77.

Ambros, V. 2001. microRNAs: tiny regulators with great potential. *Cell*. 107:823-6.

Andermann, E., J.C. Jacob, F. Andermann, S. Carpenter, L. Wolfe, and S.F. Berkovic. 1988. The Newfoundland aggregate of neuronal ceroid-lipofuscinosis. *Am J Med Genet Suppl*. 5:111-6.

Autti, T., R. Raininko, S.L. Vanhanen, and P. Santavuori. 1996. MRI of neuronal ceroid lipofuscinosis. I. Cranial MRI of 30 patients with juvenile neuronal ceroid lipofuscinosis. *Neuroradiology*. 38:476-82.

Barik, S. 2006. RNAi in moderation. *Nat Biotechnol*. 24:796-7.

Barohn, R.J., D.C. Dowd, and K.S. Kagan-Hallet. 1992. Congenital ceroid-lipofuscinosis. *Pediatr Neurol*. 8:54-9.

Batten, F. 1903. Cerebral degeneration with symmetrical changes in the maculae in two members of a family, Trans. Ophthalmol. *Soc. U. K*. 23:386–390.

Batten, F. 1914. Family cerebral degeneration with macular change (so-called juvenile form of family amaurotic idiocy). *Q.J. Med.* 7:444–454

Baulcombe, D. 2004. RNA silencing in plants. *Nature*. 431:356-63.

Becker, K., H.H. Goebel, L. Svennerholm, U. Wendel, and H.J. Bremer. 1979. Clinical, morphological, and biochemical investigations on a patient with an unusual form of neuronal ceroid-lipofuscinosis. *Eur J Pediatr*. 132:197-206.

Bielschowsky, M. 1913. Ueber spätinfantile amaurotische Idiotie mit Kleinhirnsymptomen. *Dtsch. Z. Nervenheilkd*. 50:7–29.

Bookout, A.L., C.L. Cummins, D.J. Mangelsdorf, J.M. Pesola, and M.F. Kramer. 2006. High-throughput real-time quantitative reverse transcription PCR. *Curr Protoc Mol Biol*. Chapter 15:Unit 15 8.

Brummelkamp, T.R., R. Bernards, and R. Agami. 2002. A system for stable expression of short interfering RNAs in mammalian cells. *Science*. 296:550-3.

Cai, X., K.M. Woods, S.J. Upton, and G. Zhu. 2005. Application of quantitative real-time reverse transcription-PCR in assessing drug efficacy against the intracellular pathogen Cryptosporidium parvum in vitro. *Antimicrob Agents Chemother*. 49:4437-42.

Camp, L.A., L.A. Verkruyse, S.J. Afendis, C.A. Slaughter, and S.L. Hofmann. 1994. Molecular cloning and expression of palmitoyl-protein thioesterase. *J Biol Chem*. 269:23212-9.

Cao, Y., J.A. Espinola, E. Fossale, A.C. Massey, A.M. Cuervo, M.E. MacDonald, and S.L. Cotman. 2006. Autophagy is disrupted in a knock-in mouse model of juvenile neuronal ceroid lipofuscinosis. *J Biol Chem*. 281:20483-93.

Chang, J., and J.M. Taylor. 2003. Susceptibility of human hepatitis delta virus RNAs to small interfering RNA action. *J Virol*. 77:9728-31.

Cotman, S.L., V. Vrbanac, L.A. Lebel, R.L. Lee, K.A. Johnson, L.R. Donahue, A.M. Teed, K. Antonellis, R.T. Bronson, T.J. Lerner, and M.E. MacDonald. 2002. Cln3(Deltaex7/8) knock-in mice with the common JNCL mutation exhibit progressive neurologic disease that begins before birth. *Hum Mol Genet*. 11:2709-21.

Cuervo, A.M. 2004. Autophagy: in sickness and in health. *Trends Cell Biol*. 14:70-7.

D'Incerti, L. 2000. MRI in neuronal ceroid lipofuscinosis. *Neurol Sci*. 21:S71-3.

Das, A.K., C.H. Becerra, W. Yi, J.Y. Lu, A.N. Siakotos, K.E. Wisniewski, and S.L. Hofmann. 1998. Molecular genetics of palmitoyl-protein thioesterase deficiency in the U.S. *J Clin Invest*. 102:361-70.

Dean, R.T. 1975. Direct evidence of importance of lysosomes in degradation of intracellular proteins. *Nature*. 257:414-6.

Delidow, B.C., J.J. Peluso, and B.A. White. 1989. Quantitative measurement of mRNAs by polymerase chain reaction. *Gene Anal Tech*. 6:120-4.

Ding, W.X., H.M. Ni, W. Gao, Y.F. Hou, M.A. Melan, X. Chen, D.B. Stolz, Z.M. Shao, and X.M. Yin. 2007. Differential effects of endoplasmic reticulum stress-induced autophagy on cell survival. *J Biol Chem*. 282:4702-10.

Echeverri, C.J., P.A. Beachy, B. Baum, M. Boutros, F. Buchholz, S.K. Chanda, J. Downward, J. Ellenberg, A.G. Fraser, N. Hacohen, W.C. Hahn, A.L. Jackson, A. Kiger, P.S. Linsley, L. Lum, Y. Ma, B. Mathey-Prevot, D.E. Root, D.M. Sabatini, J. Taipale, N. Perrimon, and R. Bernards. 2006. Minimizing the risk of reporting false positives in large-scale RNAi screens. *Nat Methods*. 3:777-9.

Elbashir, S.M., J. Harborth, W. Lendeckel, A. Yalcin, K. Weber, and T. Tuschl. 2001. Duplexes of 21-nucleotide RNAs mediate RNA interference in cultured mammalian cells. *Nature*. 411:494-8.

Elleder, M., J. Sokolova, and M. Hrebicek. 1997. Follow-up study of subunit c of mitochondrial ATP synthase (SCMAS) in Batten disease and in unrelated lysosomal disorders. *Acta Neuropathol*. 93:379-90.

Fearnley, I.M., J.E. Walker, R.D. Martinus, R.D. Jolly, K.B. Kirkland, G.J. Shaw, and D.N. Palmer. 1990. The sequence of the major protein stored in ovine ceroid lipofuscinosis is identical with that of the dicyclohexylcarbodiimide-reactive proteolipid of mitochondrial ATP synthase. *Biochem J*. 268:751-8.

Felbor, U., B. Kessler, W. Mothes, H.H. Goebel, H.L. Ploegh, R.T. Bronson, and B.R. Olsen. 2002. Neuronal loss and brain atrophy in mice lacking cathepsins B and L. *Proc Natl Acad Sci U S A*. 99:7883-8.

Ferrer, I., T. Arbizu, J. Pena, and J.P. Serra. 1980. A golgi and ultrastructural study of a dominant form of Kufs' disease. *J Neurol*. 222:183-90.

Fire, A., S. Xu, M.K. Montgomery, S.A. Kostas, S.E. Driver, and C.C. Mello. 1998. Potent and specific genetic interference by double-stranded RNA in Caenorhabditis elegans. *Nature*. 391:806-11.

Freeman, W.M., S.J. Walker, and K.E. Vrana. 1999. Quantitative RT-PCR: pitfalls and potential. *Biotechniques*. 26:112-22, 124-5.

Gao, H., R.M. Boustany, J.A. Espinola, S.L. Cotman, L. Srinidhi, K.A. Antonellis, T. Gillis, X. Qin, S. Liu, L.R. Donahue, R.T. Bronson, J.R. Faust, D. Stout, J.L. Haines, T.J. Lerner, and M.E. MacDonald. 2002. Mutations in a novel CLN6-encoded transmembrane protein cause variant neuronal ceroid lipofuscinosis in man and mouse. *Am J Hum Genet*. 70:324-35.

Ginzinger, D.G., T.E. Godfrey, J. Nigro, D.H. Moore, 2nd, S. Suzuki, M.G. Pallavicini, J.W. Gray, and R.H. Jensen. 2000. Measurement of DNA copy number at microsatellite loci using quantitative PCR analysis. *Cancer Res*. 60:5405-9.

Gitlin, L., S. Karelsky, and R. Andino. 2002. Short interfering RNA confers intracellular antiviral immunity in human cells. *Nature*. 418:430-4.

Gondai, T., K. Yamaguchi, N. Miyano-Kurosaki, Y. Habu, and H. Takaku. 2008. Short-hairpin RNAs synthesized by T7 phage polymerase do not induce interferon. *Nucleic Acids Res*. 36:e18.

Haltia, M. 2006. The neuronal ceroid-lipofuscinoses: from past to present. *Biochim Biophys Acta*. 1762:850-6.

Hammond, S.M. 2005. Dicing and slicing: the core machinery of the RNA interference pathway. *FEBS Lett*. 579:5822-9.

Heid, C.A., J. Stevens, K.J. Livak, and P.M. Williams. 1996. Real time quantitative PCR. *Genome Res*. 6:986-94.

Heine, C., A. Quitsch, S. Storch, Y. Martin, L. Lonka, A.E. Lehesjoki, S.E. Mole, and T. Braulke. 2007. Topology and endoplasmic reticulum retention signals of the lysosomal storage disease-related membrane protein CLN6. *Mol Membr Biol*. 24:74-87.

Heinonen, O., A. Kyttala, E. Lehmus, T. Paunio, L. Peltonen, and A. Jalanko. 2000. Expression of palmitoyl protein thioesterase in neurons. *Mol Genet Metab*. 69:123-9.

Herva, R., J. Tyynela, A. Hirvasniemi, M. Syrjakallio-Ylitalo, and M. Haltia. 2000. Northern epilepsy: a novel form of neuronal ceroid-lipofuscinosis. *Brain Pathol*. 10:215-22.

Hobert, J.A., and G. Dawson. 2007. A novel role of the Batten disease gene CLN3: association with BMP synthesis. *Biochem Biophys Res Commun*. 358:111-6.

Hofman, I.L., and P.E. Taschner. 1995. Late onset juvenile neuronal ceroid-lipofuscinosis with granular osmiophilic deposits (GROD). *Am J Med Genet*. 57:165-7.

Hughes, S.M., G.W. Kay, T.W. Jordan, G.K. Rickards, and D.N. Palmer. 1999. Disease-specific pathology in neurons cultured from sheep affected with ceroid lipofuscinosis. *Mol Genet Metab*. 66:381-6.

Jackson, A.L., S.R. Bartz, J. Schelter, S.V. Kobayashi, J. Burchard, M. Mao, B. Li, G. Cavet, and P.S. Linsley. 2003. Expression profiling reveals off-target gene regulation by RNAi. *Nat Biotechnol*. 21:635-7.

Janes, R.W., P.B. Munroe, H.M. Mitchison, R.M. Gardiner, S.E. Mole, and B.A. Wallace. 1996. A model for Batten disease protein CLN3: functional implications from homology and mutations. *FEBS Lett*. 399:75-7.

Jansk´y, J. 1908. Sur un cas jusqu´a présente non décrit de I´idiotie amaurotique familiàle compliquée par une hypoplasie du cervelet. *Sborna lék* 13:165–196.

Jarvela, I., M. Sainio, T. Rantamaki, V.M. Olkkonen, O. Carpen, L. Peltonen, and A. Jalanko. 1998. Biosynthesis and intracellular targeting of the CLN3 protein defective in Batten disease. *Hum Mol Genet*. 7:85-90.

Jolly, R.D., A. Shimada, I. Dopfmer, P.M. Slack, M.J. Birtles, and D.N. Palmer. 1989. Ceroid-lipofuscinosis (Batten's disease): pathogenesis and sequential neuropathological changes in the ovine model. *Neuropathol Appl Neurobiol*. 15:371-83.

Kariko, K., P. Bhuyan, J. Capodici, and D. Weissman. 2004. Small interfering RNAs mediate sequence-independent gene suppression and induce immune activation by signaling through toll-like receptor 3. *J Immunol*. 172:6545-9.

Kasper, D., R. Planells-Cases, J.C. Fuhrmann, O. Scheel, O. Zeitz, K. Ruether, A. Schmitt, M. Poet, R. Steinfeld, M. Schweizer, U. Kornak, and T.J. Jentsch. 2005. Loss of the chloride channel ClC-7 leads to lysosomal storage disease and neurodegeneration. *EMBO J*. 24:1079-91.

Kim, Y., D. Ramirez-Montealegre, and D.A. Pearce. 2003. A role in vacuolar arginine transport for yeast Btn1p and for human CLN3, the protein defective in Batten disease. *Proc Natl Acad Sci U S A*. 100:15458-62.

Kitzmuller, C., R.L. Haines, S. Codlin, D.F. Cutler, and S.E. Mole. 2008. A function retained by the common mutant CLN3 protein is responsible for the late onset of juvenile neuronal ceroid lipofuscinosis. *Hum Mol Genet*. 17:303-12.

Kochl, R., X.W. Hu, E.Y. Chan, and S.A. Tooze. 2006. Microtubules facilitate autophagosome formation and fusion of autophagosomes with endosomes. *Traffic*. 7:129-45.

Koike, M., M. Shibata, S. Waguri, K. Yoshimura, I. Tanida, E. Kominami, T. Gotow, C. Peters, K. von Figura, N. Mizushima, P. Saftig, and Y. Uchiyama. 2005. Participation of autophagy in storage of lysosomes in neurons from mouse models of neuronal ceroid-lipofuscinoses (Batten disease). *Am J Pathol*. 167:1713-28.

Kominami, E., J. Ezaki, and L.S. Wolfe. 1995. New insight into lysosomal protein storage disease: delayed catabolism of ATP synthase subunit c in Batten disease. *Neurochem Res*. 20:1305-9.

Kufs, H. 1925. Ueber eine spätform der amaurotischen Idiotie und ihre heredofamiliären Grundlagen, Z. Gesamte Neurol. Psychiatr. **95** (), pp. 169–188.

Kyttala, A., G. Ihrke, J. Vesa, M.J. Schell, and J.P. Luzio. 2004. Two motifs target Batten disease protein CLN3 to lysosomes in transfected nonneuronal and neuronal cells. *Mol Biol Cell*. 15:1313-23.

Kyttala, A., U. Lahtinen, T. Braulke, and S.L. Hofmann. 2006. Functional biology of the neuronal ceroid lipofuscinoses (NCL) proteins. *Biochim Biophys Acta*. 1762:920-33.

Lagos-Quintana, M., R. Rauhut, W. Lendeckel, and T. Tuschl. 2001. Identification of novel genes coding for small expressed RNAs. *Science*. 294:853-8.

Lagos-Quintana, M., R. Rauhut, A. Yalcin, J. Meyer, W. Lendeckel, and T. Tuschl. 2002. Identification of tissue-specific microRNAs from mouse. *Curr Biol*. 12:735-9.

Lake, B.D., and N.P. Cavanagh. 1978. Early-juvenile Batten's disease--a recognisable sub-group distinct from other forms of Batten's disease. Analysis of 5 patients. *J Neurol Sci*. 36:265-71.

Lander, E.S., L.M. Linton, B. Birren, C. Nusbaum, M.C. Zody, J. Baldwin, K. Devon, K. Dewar, M. Doyle, W. FitzHugh, R. Funke, D. Gage, K. Harris, A. Heaford, J. Howland, L. Kann, J. Lehoczky, R. LeVine, P.

McEwan, K. McKernan, J. Meldrim, J.P. Mesirov, C. Miranda, W. Morris, J. Naylor, C. Raymond, M. Rosetti, R. Santos, A. Sheridan, C. Sougnez, N. Stange-Thomann, N. Stojanovic, A. Subramanian, D. Wyman, J. Rogers, J. Sulston, R. Ainscough, S. Beck, D. Bentley, J. Burton, C. Clee, N. Carter, A. Coulson, R. Deadman, P. Deloukas, A. Dunham, I. Dunham, R. Durbin, L. French, D. Grafham, S. Gregory, T. Hubbard, S. Humphray, A. Hunt, M. Jones, C. Lloyd, A. McMurray, L. Matthews, S. Mercer, S. Milne, J.C. Mullikin, A. Mungall, R. Plumb, M. Ross, R. Shownkeen, S. Sims, R.H. Waterston, R.K. Wilson, L.W. Hillier, J.D. McPherson, M.A. Marra, E.R. Mardis, L.A. Fulton, A.T. Chinwalla, K.H. Pepin, W.R. Gish, S.L. Chissoe, M.C. Wendl, K.D. Delehaunty, T.L. Miner, A. Delehaunty, J.B. Kramer, L.L. Cook, R.S. Fulton, D.L. Johnson, P.J. Minx, S.W. Clifton, T. Hawkins, E. Branscomb, P. Predki, P. Richardson, S. Wenning, T. Slezak, N. Doggett, J.F. Cheng, A. Olsen, S. Lucas, C. Elkin, E. Uberbacher, M. Frazier, et al. 2001. Initial sequencing and analysis of the human genome. *Nature*. 409:860-921.

Lee, R.C., R.L. Feinbaum, and V. Ambros. 1993. The C. elegans heterochronic gene lin-4 encodes small RNAs with antisense complementarity to lin-14. *Cell*. 75:843-54.

Lehtovirta, M., A. Kyttala, E.L. Eskelinen, M. Hess, O. Heinonen, and A. Jalanko. 2001. Palmitoyl protein thioesterase (PPT) localizes into synaptosomes and synaptic vesicles in neurons: implications for infantile neuronal ceroid lipofuscinosis (INCL). *Hum Mol Genet*. 10:69-75.

Livak, K.J., and T.D. Schmittgen. 2001. Analysis of relative gene expression data using real-time quantitative PCR and the 2(-Delta Delta C(T)) Method. *Methods*. 25:402-8.

Lockhart, D.J., and E.A. Winzeler. 2000. Genomics, gene expression and DNA arrays. *Nature*. 405:827-36.

Lonka, L., A. Kyttala, S. Ranta, A. Jalanko, and A.E. Lehesjoki. 2000. The neuronal ceroid lipofuscinosis CLN8 membrane protein is a resident of the endoplasmic reticulum. *Hum Mol Genet*. 9:1691-7.

Lonka, L., T. Salonen, E. Siintola, O. Kopra, A.E. Lehesjoki, and A. Jalanko. 2004. Localization of wild-type and mutant neuronal ceroid lipofuscinosis CLN8 proteins in non-neuronal and neuronal cells. *J Neurosci Res*. 76:862-71.

Luiro, K., O. Kopra, T. Blom, M. Gentile, H.M. Mitchison, I. Hovatta, K. Tornquist, and A. Jalanko. 2006. Batten disease (JNCL) is linked to disturbances in mitochondrial, cytoskeletal, and synaptic compartments. *J Neurosci Res*. 84:1124-38.

Luiro, K., O. Kopra, M. Lehtovirta, and A. Jalanko. 2001. CLN3 protein is targeted to neuronal synapses but excluded from synaptic vesicles: new clues to Batten disease. *Hum Mol Genet*. 10:2123-31.

Luiro, K., K. Yliannala, L. Ahtiainen, H. Maunu, I. Jarvela, A. Kyttala, and A. Jalanko. 2004. Interconnections of CLN3, Hook1 and Rab proteins link Batten disease to defects in the endocytic pathway. *Hum Mol Genet*. 13:3017-27.

Margraf, L.R., R.L. Boriack, A.A. Routheut, I. Cuppen, L. Alhilali, C.J. Bennett, and M.J. Bennett. 1999. Tissue expression and subcellular localization of CLN3, the Batten disease protein. *Mol Genet Metab*. 66:283-9.

Mitchison, H.M., D.J. Bernard, N.D. Greene, J.D. Cooper, M.A. Junaid, R.K. Pullarkat, N. de Vos, M.H. Breuning, J.W. Owens, W.C. Mobley, R.M. Gardiner, B.D. Lake, P.E. Taschner, and R.L. Nussbaum. 1999. Targeted disruption of the Cln3 gene provides a mouse model for Batten disease. The Batten Mouse Model Consortium [corrected]. *Neurobiol Dis*. 6:321-34.

Mitchison, H.M., A.M. O'Rawe, P.E. Taschner, L.A. Sandkuijl, P. Santavuori, N. de Vos, M.H. Breuning, S.E. Mole, R.M. Gardiner, and I.E. Jarvela. 1995. Batten disease gene, CLN3: linkage disequilibrium mapping in the Finnish population, and analysis of European haplotypes. *Am J Hum Genet*. 56:654-62.

Mocellin, S., and M. Provenzano. 2004. RNA interference: learning gene knock-down from cell physiology. *J Transl Med*. 2:39.

Mole, S.E., R.E. Williams, and H.H. Goebel. 2005. Correlations between genotype, ultrastructural morphology and clinical phenotype in the neuronal ceroid lipofuscinoses. *Neurogenetics*. 6:107-26.

Mourelatos, Z., J. Dostie, S. Paushkin, A. Sharma, B. Charroux, L. Abel, J. Rappsilber, M. Mann, and G. Dreyfuss. 2002. miRNPs: a novel class of ribonucleoproteins containing numerous microRNAs. *Genes Dev*. 16:720-8.

Narayan, S.B., J.V. Pastor, H.M. Mitchison, and M.J. Bennett. 2004. CLN3L, a novel protein related to the Batten disease protein, is overexpressed in Cln3-/- mice and in Batten disease. *Brain*. 127:1748-54.

Narayan, S.B., D. Rakheja, L. Tan, J.V. Pastor, and M.J. Bennett. 2006. CLN3P, the Batten's disease protein, is a novel palmitoyl-protein Delta-9 desaturase. *Ann Neurol*. 60:570-7.

Nigro, J.M., M.A. Takahashi, D.G. Ginzinger, M. Law, S. Passe, R.B. Jenkins, and K. Aldape. 2001. Detection of 1p and 19q loss in oligodendroglioma by quantitative microsatellite analysis, a real-time quantitative polymerase chain reaction assay. *Am J Pathol*. 158:1253-62.

Nijssen, P.C., C. Ceuterick, O.P. van Diggelen, M. Elleder, J.J. Martin, J.L. Teepen, J. Tyynela, and R.A. Roos. 2003. Autosomal dominant adult neuronal ceroid lipofuscinosis: a novel form of NCL with granular osmiophilic deposits without palmitoyl protein thioesterase 1 deficiency. *Brain Pathol*. 13:574-81.

Nykanen, A., B. Haley, and P.D. Zamore. 2001. ATP requirements and small interfering RNA structure in the RNA interference pathway. *Cell*. 107:309-21.

Okamura, K., A. Ishizuka, H. Siomi, and M.C. Siomi. 2004. Distinct roles for Argonaute proteins in small RNA-directed RNA cleavage pathways. *Genes Dev*. 18:1655-66.

Paddison, P.J., A.A. Caudy, and G.J. Hannon. 2002. Stable suppression of gene expression by RNAi in mammalian cells. *Proc Natl Acad Sci U S A*. 99:1443-8.

Palmer, D.N., I.M. Fearnley, J.E. Walker, N.A. Hall, B.D. Lake, L.S. Wolfe, M. Haltia, R.D. Martinus, and R.D. Jolly. 1992. Mitochondrial ATP synthase subunit c storage in the ceroid-lipofuscinoses (Batten disease). *Am J Med Genet*. 42:561-7.

Palmer, D.N., R.D. Martinus, S.M. Cooper, G.G. Midwinter, J.C. Reid, and R.D. Jolly. 1989. Ovine ceroid lipofuscinosis. The major lipopigment protein and the lipid-binding subunit of mitochondrial ATP synthase have the same NH2-terminal sequence. *J Biol Chem*. 264:5736-40.

Pearce, D.A., T. Ferea, S.A. Nosel, B. Das, and F. Sherman. 1999. Action of BTN1, the yeast orthologue of the gene mutated in Batten disease. *Nat Genet*. 22:55-8.

Pearce, D.A., and F. Sherman. 1998. A yeast model for the study of Batten disease. *Proc Natl Acad Sci U S A*. 95:6915-8.

Pearce, D.A., and F. Sherman. 1999. Investigation of Batten disease with the yeast Saccharomyces cerevisiae. *Mol Genet Metab*. 66:314-9.

Persaud-Sawin, D.A., J.O. McNamara, 2nd, S. Rylova, A. Vandongen, and R.M. Boustany. 2004. A galactosylceramide binding domain is involved in trafficking of CLN3 from Golgi to rafts via recycling endosomes. *Pediatr Res.* 56:449-63.

Persaud-Sawin, D.A., T. Mousallem, C. Wang, A. Zucker, E. Kominami, and R.M. Boustany. 2007. Neuronal ceroid lipofuscinosis: a common pathway? *Pediatr Res.* 61:146-52.

Persaud-Sawin, D.A., A. VanDongen, and R.M. Boustany. 2002. Motifs within the CLN3 protein: modulation of cell growth rates and apoptosis. *Hum Mol Genet.* 11:2129-42.

Pfaffl, M.W. 2001. A new mathematical model for relative quantification in real-time RT-PCR. *Nucleic Acids Res.* 29:e45.

Philippart, M., H.T. Chugani, and J.B. Bateman. 1995. New Spielmeyer-Vogt variant with granular inclusions and early brain atrophy. *Am J Med Genet.* 57:160-4.

Pineda-Trujillo, N., W. Cornejo, J. Carrizosa, R.B. Wheeler, S. Munera, A. Valencia, J. Agudelo-Arango, A. Cogollo, G. Anderson, G. Bedoya, S.E. Mole, and A. Ruiz-Linares. 2005. A CLN5 mutation causing an atypical neuronal ceroid lipofuscinosis of juvenile onset. *Neurology.* 64:740-2.

Pohl, S., H.M. Mitchison, A. Kohlschutter, O. van Diggelen, T. Braulke, and S. Storch. 2007. Increased expression of lysosomal acid phosphatase in CLN3-defective cells and mouse brain tissue. *J Neurochem.* 103:2177-88.

Rakheja, D., S.B. Narayan, J.V. Pastor, and M.J. Bennett. 2004. CLN3P, the Batten disease protein, localizes to membrane lipid rafts (detergent-resistant membranes). *Biochem Biophys Res Commun.* 317:988-91.

Ranta, S., M. Topcu, S. Tegelberg, H. Tan, A. Ustubutun, I. Saatci, A. Dufke, H. Enders, K. Pohl, Y. Alembik, W.A. Mitchell, S.E. Mole, and A.E. Lehesjoki. 2004. Variant late infantile neuronal ceroid lipofuscinosis in a subset of Turkish patients is allelic to Northern epilepsy. *Hum Mutat.* 23:300-5.

Ranta, S., Y. Zhang, B. Ross, L. Lonka, E. Takkunen, A. Messer, J. Sharp, R. Wheeler, K. Kusumi, S. Mole, W. Liu, M.B. Soares, M.F. Bonaldo, A. Hirvasniemi, A. de la Chapelle, T.C. Gilliam, and A.E. Lehesjoki. 1999. The neuronal ceroid lipofuscinoses in human EPMR and mnd mutant mice are associated with mutations in CLN8. *Nat Genet.* 23:233-6.

Rawlings, N.D., and A.J. Barrett. 1999. Tripeptidyl-peptidase I is apparently the CLN2 protein absent in classical late-infantile neuronal ceroid lipofuscinosis. *Biochim Biophys Acta.* 1429:496-500.

Reinhart, B.J., F.J. Slack, M. Basson, A.E. Pasquinelli, J.C. Bettinger, A.E. Rougvie, H.R. Horvitz, and G. Ruvkun. 2000. The 21-nucleotide let-7 RNA regulates developmental timing in Caenorhabditis elegans. *Nature.* 403:901-6.

Rider, J.A., and D.L. Rider. 1988. Batten disease: past, present, and future. *Am J Med Genet Suppl.* 5:21-6.

Sachs, B. 1896. A family form of idiocy, generally fatal and associated with early blindness (amaurotic family idiocy), *N. Y. Med. J.* 63: 697–703.

Sadzot, B., M. Reznik, J.E. Arrese-Estrada, and G. Franck. 2000. Familial Kufs' disease presenting as a progressive myoclonic epilepsy. *J Neurol.* 247:447-54.

Santavuori, P. 1988. Neuronal ceroid-lipofuscinoses in childhood. *Brain Dev.* 10:80-3.

Santavuori, P., J. Rapola, K. Sainio, and C. Raitta. 1982. A variant of Jansky-Bielschowsky disease. *Neuropediatrics*. 13:135-41.

Savukoski, M., T. Klockars, V. Holmberg, P. Santavuori, E.S. Lander, and L. Peltonen. 1998. CLN5, a novel gene encoding a putative transmembrane protein mutated in Finnish variant late infantile neuronal ceroid lipofuscinosis. *Nat Genet*. 19:286-8.

Schneeberger, C., P. Speiser, F. Kury, and R. Zeillinger. 1995. Quantitative detection of reverse transcriptase-PCR products by means of a novel and sensitive DNA stain. *PCR Methods Appl*. 4:234-8.

Schulz, A., S. Dhar, S. Rylova, G. Dbaibo, J. Alroy, C. Hagel, I. Artacho, A. Kohlschutter, S. Lin, and R.M. Boustany. 2004. Impaired cell adhesion and apoptosis in a novel CLN9 Batten disease variant. *Ann Neurol*. 56:342-50.

Schulz, A., T. Mousallem, M. Venkataramani, D.A. Persaud-Sawin, A. Zucker, C. Luberto, A. Bielawska, J. Bielawski, J.C. Holthuis, S.M. Jazwinski, L. Kozhaya, G.S. Dbaibo, and R.M. Boustany. 2006. The CLN9 protein, a regulator of dihydroceramide synthase. *J Biol Chem*. 281:2784-94.

Seehafer, S.S., and D.A. Pearce. 2006. You say lipofuscin, we say ceroid: defining autofluorescent storage material. *Neurobiol Aging*. 27:576-88.

Semizarov, D., L. Frost, A. Sarthy, P. Kroeger, D.N. Halbert, and S.W. Fesik. 2003. Specificity of short interfering RNA determined through gene expression signatures. *Proc Natl Acad Sci U S A*. 100:6347-52.

Shannon, K.E., D.Y. Lee, J.T. Trevors, and L.A. Beaudette. 2007. Application of real-time quantitative PCR for the detection of selected bacterial pathogens during municipal wastewater treatment. *Sci Total Environ*. 382:121-9.

Siintola, E., S. Partanen, P. Stromme, A. Haapanen, M. Haltia, J. Maehlen, A.E. Lehesjoki, and J. Tyynela. 2006. Cathepsin D deficiency underlies congenital human neuronal ceroid-lipofuscinosis. *Brain*. 129:1438-45.

Siintola, E., M. Topcu, N. Aula, H. Lohi, B.A. Minassian, A.D. Paterson, X.Q. Liu, C. Wilson, U. Lahtinen, A.K. Anttonen, and A.E. Lehesjoki. 2007. The novel neuronal ceroid lipofuscinosis gene MFSD8 encodes a putative lysosomal transporter. *Am J Hum Genet*. 81:136-46.

Sijen, T., and R.H. Plasterk. 2003. Transposon silencing in the Caenorhabditis elegans germ line by natural RNAi. *Nature*. 426:310-4.

Sleat, D.E., R.J. Donnelly, H. Lackland, C.G. Liu, I. Sohar, R.K. Pullarkat, and P. Lobel. 1997. Association of mutations in a lysosomal protein with classical late-infantile neuronal ceroid lipofuscinosis. *Science*. 277:1802-5.

Sledz, C.A., M. Holko, M.J. de Veer, R.H. Silverman, and B.R. Williams. 2003. Activation of the interferon system by short-interfering RNAs. *Nat Cell Biol*. 5:834-9.

Spielmeyer, W. 1905. Ueber familiäre amaurotische Idiotien. *Neurol. Cbl*. 24:620–621.

Spielmeyer, W. 1905. Weitere Mittheilung ueber eine besondere Form von familiärer amaurotischer Idiotie. *Neurol. Cbl*. 24:1131–1132.

Spielmeyer, W. 1908. Klinische und anatomische Untersuchungen ueber eine besondere Form von familiärer amaurotischer Idiotie. *Histol. Histopathol*. 2:193–251.

Stark, G.R., I.M. Kerr, B.R. Williams, R.H. Silverman, and R.D. Schreiber. 1998. How cells respond to interferons. *Annu Rev Biochem*. 67:227-64.

Stengel, C. 1826. Beretning om et maerkeligt Sygdomstilfaelde hos fire Soedskende i Naerheden af Roeraas. Eyr et medicinsk Tidskrift. 1:347–352.

Steinfeld, R., K. Reinhardt, K. Schreiber, M. Hillebrand, R. Kraetzner, W. Bruck, P. Saftig, and J. Gartner. 2006. Cathepsin D deficiency is associated with a human neurodegenerative disorder. *Am J Hum Genet*. 78:988-98.

Taira, T., Y. Saito, T. Niki, S.M. Iguchi-Ariga, K. Takahashi, and H. Ariga. 2004. DJ-1 has a role in antioxidative stress to prevent cell death. *EMBO Rep*. 5:213-8.

Tang, C.H., J.W. Lee, M.G. Galvez, L. Robillard, S.E. Mole, and H.A. Chapman. 2006. Murine cathepsin F deficiency causes neuronal lipofuscinosis and late-onset neurological disease. *Mol Cell Biol*. 26:2309-16.

Tang, J., and R.N. Wong. 1987. Evolution in the structure and function of aspartic proteases. *J Cell Biochem*. 33:53-63.

The International Batten Disease Consortium. 1995. Isolation of a novel gene underlying Batten disease, CLN3. *Cell*. 82:949-57.

Topcu, M., H. Tan, D. Yalnizoglu, A. Usubutun, I. Saatci, M. Aynaci, B. Anlar, H. Topaloglu, G. Turanli, G. Kose, and S. Aysun. 2004. Evaluation of 36 patients from Turkey with neuronal ceroid lipofuscinosis: clinical, neurophysiological, neuroradiological and histopathologic studies. *Turk J Pediatr*. 46:1-10.

Tsai, S.J., and M.C. Wiltbank. 1996. Quantification of mRNA using competitive RT-PCR with standard-curve methodology. *Biotechniques*. 21:862-6.

Tyynela, J., D.N. Palmer, M. Baumann, and M. Haltia. 1993. Storage of saposins A and D in infantile neuronal ceroid-lipofuscinosis. *FEBS Lett*. 330:8-12.

Tyynela, J., J. Suopanki, P. Santavuori, M. Baumann, and M. Haltia. 1997. Variant late infantile neuronal ceroid-lipofuscinosis: pathology and biochemistry. *J Neuropathol Exp Neurol*. 56:369-75.

Uvebrant, P., and B. Hagberg. 1997. Neuronal ceroid lipofuscinoses in Scandinavia. Epidemiology and clinical pictures. *Neuropediatrics*. 28:6-8.

van Diggelen, O.P., S. Thobois, C. Tilikete, M.T. Zabot, J.L. Keulemans, P.A. van Bunderen, P.E. Taschner, M. Losekoot, and Y.V. Voznyi. 2001. Adult neuronal ceroid lipofuscinosis with palmitoyl-protein thioesterase deficiency: first adult-onset patients of a childhood disease. *Ann Neurol*. 50:269-72.

Venter, J.C., M.D. Adams, E.W. Myers, P.W. Li, R.J. Mural, G.G. Sutton, H.O. Smith, M. Yandell, C.A. Evans, R.A. Holt, J.D. Gocayne, P. Amanatides, R.M. Ballew, D.H. Huson, J.R. Wortman, Q. Zhang, C.D. Kodira, X.H. Zheng, L. Chen, M. Skupski, G. Subramanian, P.D. Thomas, J. Zhang, G.L. Gabor Miklos, C. Nelson, S. Broder, A.G. Clark, J. Nadeau, V.A. McKusick, N. Zinder, A.J. Levine, R.J. Roberts, M. Simon, C. Slayman, M. Hunkapiller, R. Bolanos, A. Delcher, I. Dew, D. Fasulo, M. Flanigan, L. Florea, A. Halpern, S. Hannenhalli, S. Kravitz, S. Levy, C. Mobarry, K. Reinert, K. Remington, J. Abu-Threideh, E. Beasley, K. Biddick, V. Bonazzi, R. Brandon, M. Cargill, I. Chandramouliswaran, R. Charlab, K. Chaturvedi, Z. Deng, V. Di Francesco, P. Dunn, K. Eilbeck, C. Evangelista, A.E. Gabrielian, W. Gan, W. Ge, F. Gong, Z. Gu, P. Guan, T.J. Heiman, M.E. Higgins, R.R. Ji, Z. Ke, K.A. Ketchum, Z. Lai, Y. Lei, Z. Li, J. Li, Y. Liang, X. Lin, F. Lu, G.V. Merkulov, N. Milshina, H.M. Moore,

A.K. Naik, V.A. Narayan, B. Neelam, D. Nusskern, D.B. Rusch, S. Salzberg, W. Shao, B. Shue, J. Sun, Z. Wang, A. Wang, X. Wang, J. Wang, M. Wei, R. Wides, C. Xiao, C. Yan, et al. 2001. The sequence of the human genome. *Science*. 291:1304-51.

Verkruyse, L.A., and S.L. Hofmann. 1996. Lysosomal targeting of palmitoyl-protein thioesterase. *J Biol Chem*. 271:15831-6.

Vesa, J., M.H. Chin, K. Oelgeschlager, J. Isosomppi, E.C. DellAngelica, A. Jalanko, and L. Peltonen. 2002. Neuronal ceroid lipofuscinoses are connected at molecular level: interaction of CLN5 protein with CLN2 and CLN3. *Mol Biol Cell*. 13:2410-20.

Vesa, J., E. Hellsten, L.A. Verkruyse, L.A. Camp, J. Rapola, P. Santavuori, S.L. Hofmann, and L. Peltonen. 1995. Mutations in the palmitoyl protein thioesterase gene causing infantile neuronal ceroid lipofuscinosis. *Nature*. 376:584-7.

Vogt, H. 1905. Ueber familiäre amaurotische Idiotie und verwandte Krankheitsbilder. *Mschr. Psychiatr. Neurol.* 19:161–171.

Vogt, H. 1907. Zur Pathologie und pathologischen Anatomie der verschiedenen Idiotie-Formen. *Mschr. Psychiatr. Neurol*. 22:403–418.

Vogt, H. 1909. Familiäre amaurotische Idiotie. Histologische und histopathologische Studien. *Arch. Kinderheilkd.* 51:1–35.

Wheeler, R.B., J.D. Sharp, R.A. Schultz, J.M. Joslin, R.E. Williams, and S.E. Mole. 2002. The gene mutated in variant late-infantile neuronal ceroid lipofuscinosis (CLN6) and in nclf mutant mice encodes a novel predicted transmembrane protein. *Am J Hum Genet*. 70:537-42.

Wightman, B., I. Ha, and G. Ruvkun. 1993. Posttranscriptional regulation of the heterochronic gene lin-14 by lin-4 mediates temporal pattern formation in C. elegans. *Cell*. 75:855-62.

Winter, E., and C.P. Ponting. 2002. TRAM, LAG1 and CLN8: members of a novel family of lipid-sensing domains? *Trends Biochem Sci*. 27:381-3.

Wisniewski, K.E., A. Kaczmarski, E. Kida, F. Connell, W. Kaczmarski, M.P. Michalewski, D.N. Moroziewicz, and N. Zhong. 1999. Reevaluation of neuronal ceroid lipofuscinoses: atypical juvenile onset may be the result of CLN2 mutations. *Mol Genet Metab*. 66:248-52.

Wlodawer, A., M. Li, A. Gustchina, Z. Dauter, K. Uchida, H. Oyama, N.E. Goldfarb, B.M. Dunn, and K. Oda. 2001. Inhibitor complexes of the Pseudomonas serine-carboxyl proteinase. *Biochemistry*. 40:15602-11.

Yoo, J.W., S. Kim, and D.K. Lee. 2008. Competition potency of siRNA is specified by the 5'-half sequence of the guide strand. *Biochem Biophys Res Commun*. 367:78-83.

Yoshikawa, M., S. Uchida, J. Ezaki, T. Rai, A. Hayama, K. Kobayashi, Y. Kida, M. Noda, M. Koike, Y. Uchiyama, F. Marumo, E. Kominami, and S. Sasaki. 2002. CLC-3 deficiency leads to phenotypes similar to human neuronal ceroid lipofuscinosis. *Genes Cells*. 7:597-605.

Zelnik, N., M. Mahajna, T.C. Iancu, R. Sharony, and M. Zeigler. 2007. A novel mutation of the CLN8 gene: is there a Mediterranean phenotype? *Pediatr Neurol*. 36:411-3.

Zeman, W., and P. Dyken. 1969. Neuronal ceroid-lipofuscinosis (Batten's disease): relationship to amaurotic family idiocy? *Pediatrics*. 44:570-83.

APPENDIX 1

JCB-Abbreviation Standards

2D, two-dimensional
3D, three-dimensional

A, ampere
  µA, microampere(s)
  mA, milliampere(s)
Å, angstrom (10^{-10} m)
aa, amino acid(s)
ACTH, adrenocorticotropin
ADP, adenosine diphosphate
AMP, adenosine monophosphate
  cAMP, cyclic AMP
AP, alkaline phosphatase
ATP, adenosine triphosphate
ATPase, adenosine triphosphatase

BHK, baby hamster kidney
bp, base pair
BrdU, bromodeoxyuridine
BSA, bovine serum albumin

°C, degree Celsius
CaM, calmodulin
Cdk, cyclin-dependent kinase
CFP, cyan fluorescent protein
CHAPS, 3-(3-cholamidopropyl) diethy-ammonio-1 propanesulfonate
CHO, Chinese hamster ovary
Ci, curie(s)
  µCi, microcurie(s)
  mCi, millicurie(s)
Con A, concanavalin A
cpm, counts per minute
cps, counts per second
CTP, cytidine triphosphate
cycle/min, cycle(s) per minute
cycle/s, cycle(s) per second

D, dalton
d, day
d, density
DAB, diaminobenzidine
DAG, diacylglycerol
DAPI, 6'-diamidino-2 phenylindole
DEAE, diethylaminoethyl
diam, diameter
DME, Dulbecco's modified Eagle's medium
DMSO, dimethyl sulfoxide
DNA, deoxyribonucleic acid
  cDNA, complementary DNA
DNase, deoxyribonuclease
DNP, dinitrophenyl
dpm, disintegrations per minute
dps, disintegrations per second
DTT, dithiothreitol

ECL, enhanced chemiluminescence
ECM, extracellular matrix
EDTA, ethylenediaminetetraacetic acid
EGF, epidermal growth factor
EGFP, enhanced GFP
EGTA, ethyleneglycol-bis (beta-aminoethylether)- *N,N'*-tetraacetic acid
ELISA, enzyme-linked immunosorbent assay
EM, electron microscopy
ER, endoplasmic reticulum
EST, expressed sequence tag

°F, degree Fahrenheit
FACS, BD fluorescence-activated cell sorter
FAK, focal adhesion kinase F-actin, filamentous actin
FBS, fetal bovine serum
FCS, fetal calf serum
FGF, fibroblast growth factor
FISH, fluorescent in situ hybridization
FITC, fluorescein isothiocyanate
FRAP, fluorescence recovery after photobleaching

g, gram
g, unit of gravity
GDP, guanosine diphosphate
GFP, green fluorescent protein
GST, glutathione *S*-transferase
GTP, guanosine triphosphate
GTPase, guanosine triphosphatase

h, hour
HA, hemagglutinin
HBSS, Hanks' balanced salt solution
Hepes, *N*-2-hydroxyethylpiperazine-*N'*-2-ethane sulfonic acid
HPLC, high performance liquid chromatography
HRP, horseradish peroxidase

IEF, isoelectric focusing
IFN, interferon
Ig, immunoglobulin
i.l., intraluminal(ly)
i.m., intramuscular(ly)
i.p., intraperitoneal(ly)
IPTG, isopropyl-ß-D-thiogalactoside
IU, international unit(s)
i.v., intravenous(ly)

JNK, c-Jun NH_2-terminal kinase

kb, kilobase(s)
kbp, kilobase pair(s)
kD, kilodalton(s)

liter(s), liter(s)
  µl, microliter(s)
  ml, milliliter(s)

m, meter
  µm, micrometer(s)

M, molar
mAb, monoclonal antibody
MAPK, mitogen-activated protein kinase
MDCK, Madin-Darby canine kidney
MEM, Eagle's minimum essential medium
MES, 2-(*N*-morpholino)ethane sulfonic acid
min, minute
mo, month
MOI, multiplicity of infection
mol, mole(s)
mol wt, molecular weight
MOPS, morpholino propane sulfonic acid
M_r, relative molecular mass

N, normal (concentration of ionizable groups)
n, number in a study or group
NA, numerical aperture
NAD^+, nicotinamide adenine dinucleotide
NADH, NAD^+ reduced
NADP, NAD^+phosphate
NADPH, NADP reduced
NBD, nitrobenzoxadiazole
ND, not determined
NEPHGE, nonequilibrium pH gradient electrophoresis
NGF, nerve growth factor
NLS, nuclear localization signal
No., number
NP-40, Nonidet P-40
NS, not significant
NSF, N-ethyl-maleimide sensitive fusion protein
nt, nucleotide

OD, optical density
ORF, open reading frame
osM, osmolar

PAGE, polyacrylamide gel electrophoresis
PBS, phosphate-buffered saline
PCA, perchloric acid
PCR, polymerase chain reaction
PDGF, platelet-derived growth factor
PFA, paraformaldehyde
P_i, inorganic orthophosphate
Pipes, [1,4-piperazinebis(ethane sulfonic acid)]
PKC, protein kinase C
PLC, phospholipase C
PMA, phorbol myristate acetate
PMSF, phenylmethylsulfonyl fluoride

r, correlation coefficient
RBC, red blood cell
RER, rough endoplasmic reticulum
RIA, radioimmunoassay
RNA, ribonucleic acid
  mRNA, messenger RNA
  siRNA, small interfering RNA
  tRNA, transfer RNA
RNAi, RNA interference
RNase, ribonuclease
RNP, ribonucleoprotein
rpm, revolutions per minute
RT, room temperature
RT-PCR, reverse transcription PCR

s, seconds(s)
s, sedimentation coefficient
S, Svedberg unit of sedimentation coefficient
SD, standard deviation
SDS, sodium dodecyl sulfate
SEM, standard error of the mean
SNAP, soluble NSF attachment protein
SNARE, SNAP receptor
sp act, specific activity
SSC, standard saline citrate
SV40, simian virus 40

t test, Student's *t* test
$t_{1/2}$, half-life, half-time
TBS, Tris-buffered saline
TCA, trichloroacetic acid
TdR, thymidine deoxyribose
TGF, transforming growth factor
TGN, *trans*-Golgi network
TLC, thin layer chromatography
TNF, tumor necrosis factor
TRITC, tetramethylrhodamine isothiocyanate
Tris, tris(hydroxymethyl)aminomethane
t-SNARE, target membrane SNARE
TUNEL, Tdt-mediated dUTP-biotin nick end labeling

U, unit
UDP, uridine diphosphate
UTP, uridine triphosphate
UV, ultraviolet

V, volt
VEGF, vascular endothelial growth factor
vol, volume
v-SNARE, vesicle membrane SNARE

W, watt
WGA, wheat germ agglutinin
wk, week
wt, weight

YFP, yellow fluorescent protein
yr, year